

27. IGNEOUS GEOCHEMISTRY AND PETROGENESIS OF THE IZU-BONIN FOREARC BASIN¹

Rex N. Taylor,² Henriette Lapiere,³ Phillippe Vidal,⁴ Robert W. Nesbitt,² and Ian W. Croudace²

ABSTRACT

Major element, trace element, and radiogenic isotope compositions of samples collected from Ocean Drilling Program Leg 126 in the Izu-Bonin forearc basin are presented. Lavas from the center of the basin (Site 793) are high-MgO, low-Ti, two-pyroxene basaltic andesites, and represent the products of synrift volcanism in the forearc region. These synrift lavas share many of the geochemical and petrographic characteristics of boninites. In terms of their element abundances, ratios, and isotope systematics they are intermediate between low-Ti arc tholeiites from the active arc and boninites of the outer-arc high. These features suggest a systematic geochemical gradation between volcanics related to trench distance and a variably depleted source.

A basement high drilled on the western flank of the basin (Site 792) comprises a series of plagioclase-rich two-pyroxene andesites with calc-alkaline affinities. These lavas are similar to calc-alkaline volcanics from Japan, but have lower contents of Ti, Zr, and low-field-strength elements (LFSE).

Lavas from Site 793 show inter-element variations between Zr, Ti, Sr, Ni, and Cr that are consistent with those predicted during crystallization and melting processes. In comparison, concentrations of P, Y, LFSE, and the rare-earth elements (REE) are anomalous. These elements have been redistributed within the lava pile, concentrating particularly in sections of massive and pillowed flows. Relative movement of these two-element groupings can be related to the alteration of interstitial basaltic andesite glass to a clay mineral assemblage by a post-eruptive process. Fluid-rock interaction has produced similar effects in the basement lavas of Site 792. In this sequence, andesites and dacites have undergone a volume change related to silica mobility. As a result of this process, some lithologies have the major element characteristics of basaltic andesite and rhyolite, but can be related to andesitic or dacitic precursors by silica removal or addition.

INTRODUCTION

The Izu-Bonin arc-trench system is the product of about 50 Ma of Pacific lithosphere subduction. Magmatism during this time has periodically shifted from forearc to arc and backarc during arc-chain and rift-basin development, creating distinct volcanotectonic units. One of the aims of Leg 126 was to investigate the origin, timing, and products of the Izu-Bonin forearc rift-basin. The forearc basin is 40–80 km across and can be traced as a basement feature for 2000 km from south of Japan to east of Guam aside the Izu, Volcano, and Mariana arcs. Drilling results from Leg 126 have shown that this basin initiated during the Oligocene (about 30–32 Ma) by the stretching of formerly contiguous outer-arc high and remnant arc terranes of Eocene and early Oligocene age (Leg 126 Shipboard Scientific Party, 1989a; 1989b). The basin was rapidly filled by volcanoclastic material derived from the uplifted blocks (Taylor, Fujioka, et al., 1990), which produced the 1–4-km-thick sedimentary cover.

To investigate the nature of the previously unsampled basement flooring the Izu-Bonin forearc basin, two deep holes were drilled through the sedimentary fill (Figs. 1 and 2). The first, Hole 793B, penetrated 1404 m of sediment in the center of the basin before entering volcanic basement. In addition to basement, igneous material was recovered from a Neogene sill in Hole 793B and as clasts within the coarser volcanoclastic units. The second, Hole 792E, was located on a frontal-arc high in the west of the forearc basin (Figs. 1 and 2) and reached basement at 804 mbsf. This study details the petrology and geochemistry of the igneous units recovered from the forearc, and discusses their petrogenesis and significance within the framework of intraoceanic arc evolution.

SITE 793

Rift Volcanism in the Forearc

Constraints from multichannel seismic surveys and Leg 126 drilling have shown that the Izu-Bonin forearc basin was initiated during the middle to late Oligocene (Taylor and Mitchell, this volume). Rifting of the Eocene basement, presently exposed on the Bonin Islands and recovered at Site 786 (ODP Leg 125; Fryer, Pearce, Stokking, et al., 1990), produced a series of half-graben structures on the eastern flank of the basin. Oligocene turbidites rapidly filled these structures and lapped onto footwall basement of the outer-arc high. Late Oligocene–Miocene strata show a decline in sedimentation rates with deposition of more calcareous and fine-grained facies. Renewed arc activity between 6 Ma and the present is recorded in the Pliocene/Quaternary strata as mixtures of scoriaceous and pumiceous sands and gravels. Growth of the currently active volcanic edifices is also displayed as a downwarp of seismic reflectors toward the arc volcanoes. This is caused in part by the loading effect of the developing volcanic mass on the thin arc crust (Taylor et al., 1990).

Volcanic Stratigraphy

Beneath the forearc basin sediments, Hole 793B penetrated 279 m of volcanic basement, consisting of intercalated volcanic breccias (65%), pillowed flows (15%), and massive flows (20%), as illustrated in Figure 3. The volcanic breccias are predominantly monolithic, containing clasts of pillow and massive flow of similar compositions to the adjacent lavas. The matrix to these clasts consists of relict glass shards, fine lava debris, and phenocrysts. Clast sorting and heterolithic fragments within the uppermost breccia (Unit 1) indicate local reworking of the volcanoclastic material.

The basement sequence represents the product of a submarine-rift volcano. The high proportion of volcanic breccias can be related to synvolcanic half-graben faulting, which would provide a number of unstable scarps along which volcanic debris and lava flows could accumulate. The Unit 1 breccia represents a decline in volcanic activity and a change from locally derived clastic

¹ Taylor, B., Fujioka, K., et al., 1992, *Proc. ODP, Sci. Results*, 126: College Station, TX (Ocean Drilling Program).

² Department of Geology, The University of Southampton, Southampton, SO9 5NH, United Kingdom.

³ URA-CNRS 1366, 69, Université Joseph Fourier, Institut Dolomieu, 15 Rue Maurice Gignoux, 38031 Grenoble Cedex, France.

⁴ Unité Associée no. 10, CNRS et Université Blaise Pascal, Clermont-Ferrand, France.

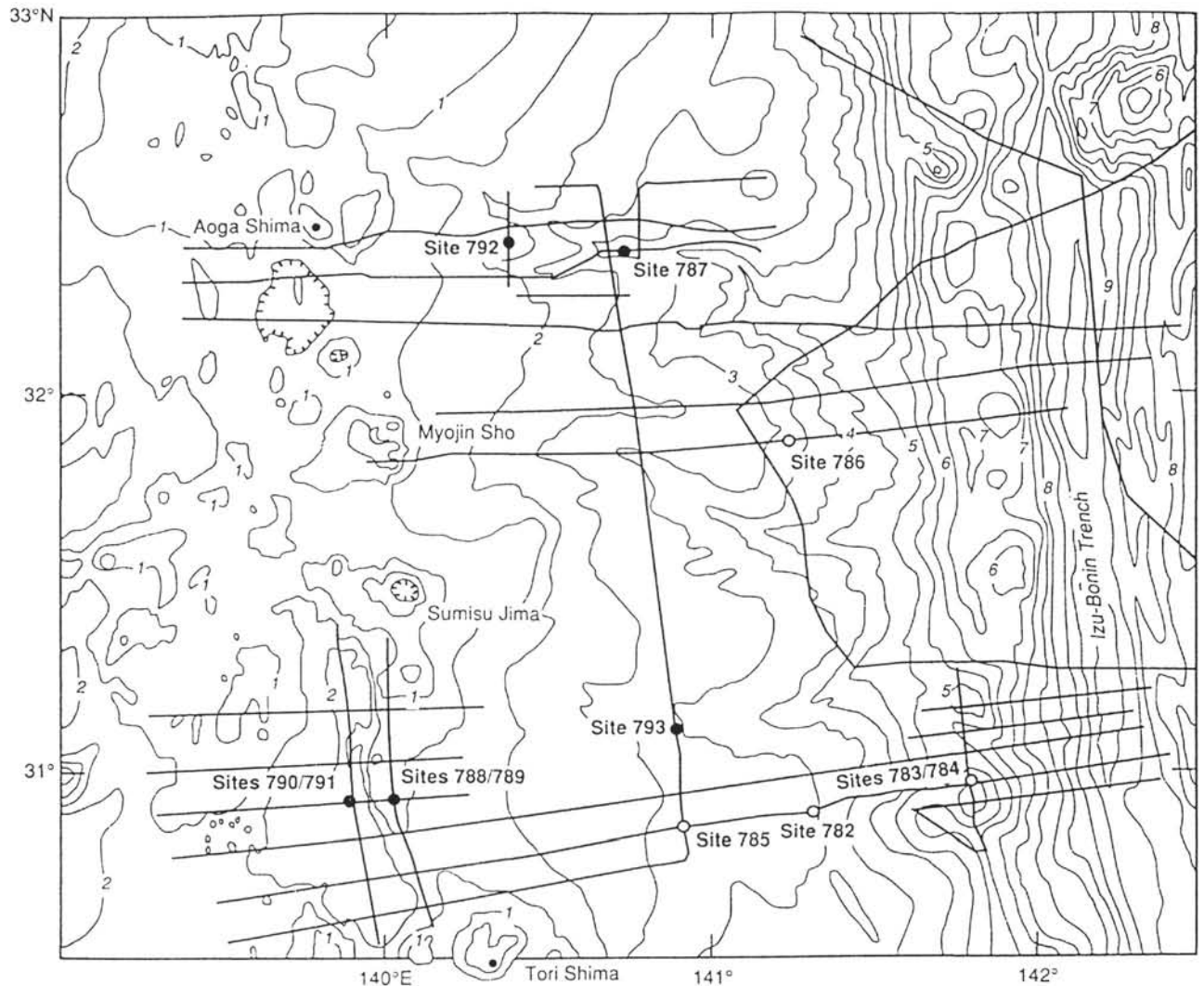


Figure 1. Bathymetric map of the Izu-Bonin arc-trench system between 30.5° and 33°N. The locations of sites drilled on Legs 125 (open circles) and 126 (solid circles) are shown on the map as are the locations of site survey multichannel seismic lines. Contour interval = 500 m (numbers on contour lines indicate depth in km). From Taylor, Fujioka, et al. (1990).

deposition into the more distal, coarse-clastic sedimentation during further basinal stretching.

Petrography

The transition from sedimentary sequence to basement is marked by a change from volcanogenic conglomerates to a heterolithic volcanic breccia. The most apparent distinction between these units in the recovered material was the presence of highly plagioclase-phyric andesites in the sediments and pyroxene-phyric lavas in the breccia. This distinction was amplified by the petrographic study of clast material in the conglomerates and breccia. Figure 3 shows the change in phenocryst assemblage between cover and basement. The clasts in sedimentary Unit V have a plagioclase-clinopyroxene-orthopyroxene-magnetite (plag-cpx-opx-mgte) crystallization assemblage, similar to the calc-alkaline andesites recovered in Hole 792E (see below). In contrast, the basement volcanics show crystallization of the pyroxenes before plagioclase (ol-opx + cpx-plag) and magnetite is either absent or limited to the groundmass.

Basement lavas and breccia clasts are composed of four phenocryst assemblages (listed below in approximate abundance order) distributed randomly throughout the stratigraphy (see Fig. 3 and Table 1):

- (i) cpx + opx + olivine (ol) + chrome spinel (porphyritic)
- (ii) cpx + opx (porphyritic)
- (iii) cpx + opx + plag (porphyritic)
- (iv) cpx + plag (aphyric)

Type (iii) is the dominant assemblage in the stratigraphy. The mineral chemistry from Hole 793B basement is discussed in a parallel contribution (Lapierre et al., this volume). A typical texture from a Type (i) lava is shown in Plate 1, and brief details of the phenocryst minerals follow.

Olivine

Only represented by saponite/celadonite/hematite/calcite pseudomorphs after subhedral or anhedral grains, with inclusions of chrome

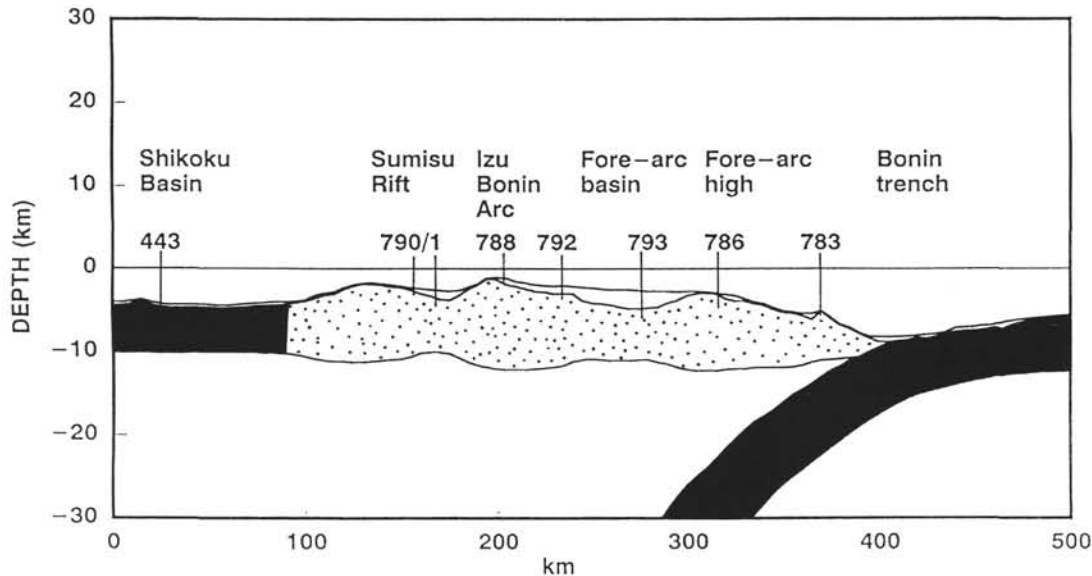


Figure 2. Schematic west-east section across the Izu-Bonin arc-trench system. Numbers refer to DSDP and ODP sites. Shaded regions are MORB-type crust; stippled regions are arc-related crust.

spinel. Unit 13 (Orange Spot flow) contains about 8% olivine pseudomorphs arranged as glomeroporphyritic clots.

Clinopyroxene

Present as fresh phenocrysts in all units of the basement. Euhedral-subhedral crystals are 1–10 mm in size, occasionally are twinned, and have minor compositional zoning. Compositions range from $\text{En}_{39}:\text{Wo}_{44}:\text{Fs}_{17}$ to $\text{En}_{54}:\text{Wo}_{39}:\text{Fs}_7$.

Orthopyroxene

Occurs as euhedral-subhedral phenocrysts 1–5 mm in size. Crystal margins and sometimes whole crystals are replaced by smectite and celadonite. Limited compositional zoning is present, but rims tend to be slightly more Fe-rich. Compositions range from En_{82} to En_{88} .

Plagioclase

Subhedral, fresh phenocrysts 0.3–2 mm in size. Compositions vary from An_{64} to An_{90} between phenocrysts, and from An_{60} to An_{86} in the laths and microlites of the groundmass.

Geochemistry

Major and trace element analyses were undertaken on 86 samples from the basement volcanics and lava clasts from the lowest 350 m of Hole 793B (Table 2). A Philips PW1400 fully automatic X-ray fluorescence spectrometer fitted with a 3 kW Rh anode tube was used for the analysis of all samples at the Department of Geology, University of Southampton. Major elements were obtained from fusion beads prepared from 1 g calcined rock powder and 5 g of Spectroflux 100B. Matrix effects were compensated for by using Philips' alphas (influence coefficients). Precision and accuracy are both high and nominally better than 1% (relative). Loss on ignition (LOI) was measured for each sample as the weight lost on samples between 100°C and 1000°C, and is excluded from the totals reported in Tables 2, 5, and 7.

Trace elements were determined on 40 mm diameter powder pellets pressed to 10 tonnes. Twelve drops of an 8% w/v aqueous solution of polyvinyl alcohol were used as a binder. Corrections for

matrix effects for trace elements were made for all wavelength regions, using the Compton scatter technique (full procedural details can be found in Croudace and Gilligan, 1990). Modified corrections, necessary when crossing absorption edges, were also applied to Ba, V, and Cr. Concentration calibrations were performed using carefully chosen high-quality geological reference samples (basic-intermediate composition). Precision and accuracy are generally better than 1% (relative), when the element concentrations are well above their detection limits. Detection limits are approximately 1 ppm for Zr, Nb, Y, Ga, Rb, Sr, Ni, Cu, and Zn and 6 ppm for Cr, V, and Ba.

Phosphorus was measured both on fusion beads and powder pellets, although the latter data are preferred because the determinations are considerably more sensitive and precise. Using powder pellets, all samples were counted by recycling the measurements six times, and counting at peak and background positions for 200 and 100 s, respectively. Matrix corrections were applied using mass absorption coefficients calculated from major element compositions. Precision is better than 2% rel. at 100 ppm P.

Major and Trace Element Systematics

In Figure 4, major elements (recalculated anhydrous) are plotted against MgO for the basement volcanics. Negative correlations exist with Al_2O_3 and TiO_2 , whereas CaO and Fe_2O_3 remain roughly constant with decreasing MgO. The plots in Figure 4 include the fields for phenocryst compositions, a bulk extract (B) composition (a composition weighted according to the average modal proportions of phenocrystal minerals present in lavas with >7 wt% MgO), and a bulk-extract control line.

The major element plots demonstrate that the majority of whole-rock compositions can be interrelated by the removal or addition of the bulk extract composition. This relationship is pursued further by least-squares mixing calculations (Table 3). These calculations confirm that extracting the observed modal proportions in a quantity equivalent to phenocryst abundances successfully links the whole-rock compositions. As such, it is possible that groundmass or liquid compositions were similar throughout the majority of lavas, with phenocryst abundance causing whole-rock variations. This notion is supported by the lack of variation in clinopyroxene and plagioclase chemistry from lavas with widely varying MgO contents (Lapierre et al., this volume).

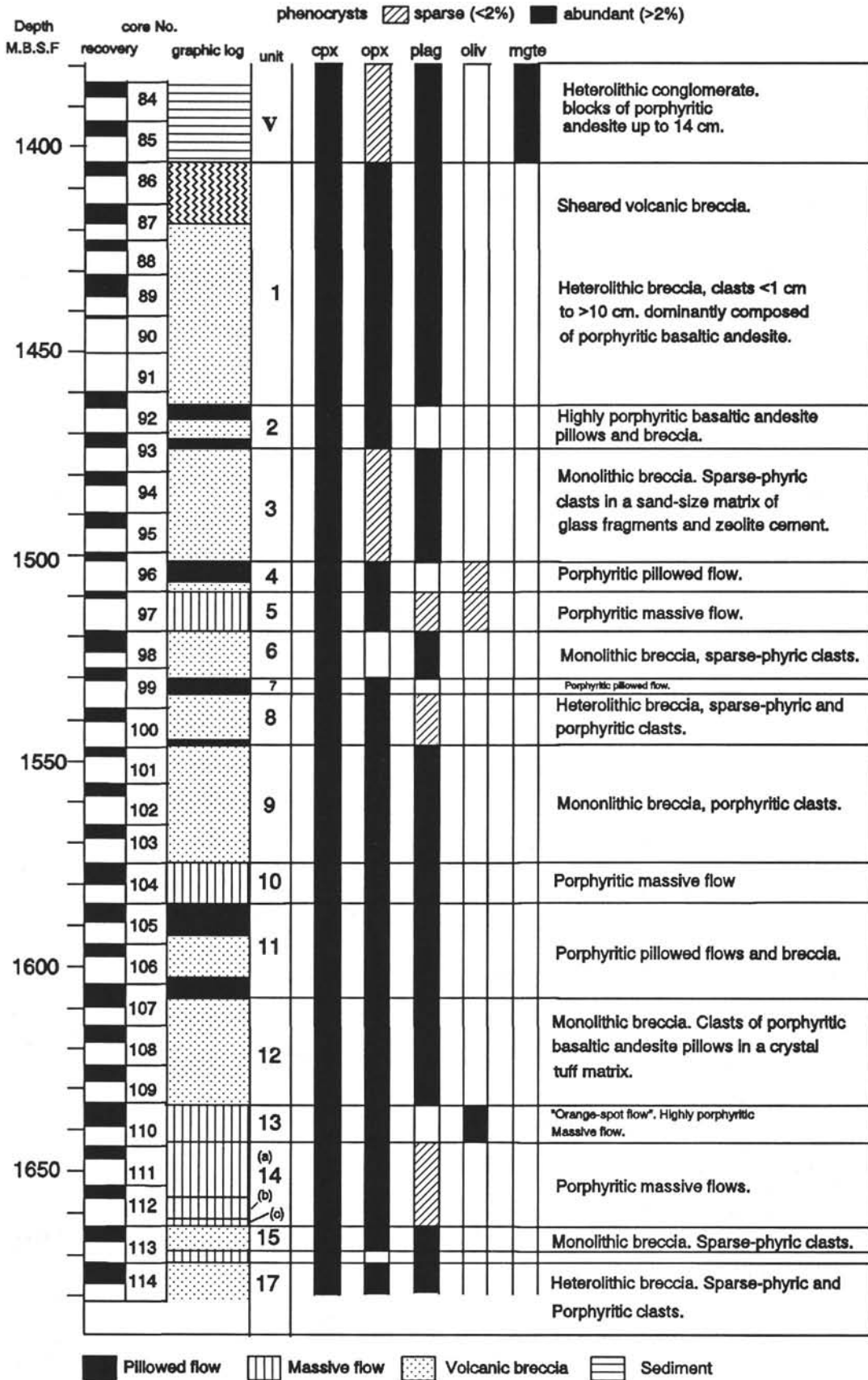


Figure 3. Basement stratigraphy, Hole 793B. Phenocryst assemblage throughout the stratigraphy is shown in the columns on right. Shaded = abundant (>2% modal), hatched = sparse (<2%), blank = absent. Abbreviations: cpx = clinopyroxene, opx = orthopyroxene, plag = plagioclase, olv = olivine, and mgte = magnetite/opaue.

Table 1. Modal mineralogy of basement rocks, Hole 793B.

Sample/analysis	Core, section, interval (cm)	Depth (mbsf)	Unit	Cpx	Opx	Plag	Oliv	Vesic	Petrological type
044	97R-1, 80	1515.78	5	10.5	5.9	0.9	1.2	4.3	(i)
S-19	110R-1, 1	1633.83	13	8.8	7.8	0.1	8.4	0.7	(i)
030	92R-2, 70	1465.32	2	23.5	16.7	0.3	—	2.7	(ii)
083	112R-2, 57	1661.38	14	16.6	12.2	0.5	—	2.9	(ii)
053	104R-1, 65	1577.11	10	13.8	3.1	7.4	—	3.7	(iii)
051	102R-1, 128	1562.51	9	1.6	2.5	3.2	—	6.5	(iii)
058	105R-1	1585.61	11	7.8	11.7	9.4	—	5.4	(iii)
033	92R-3, 55	1468.50	2	6.1	6.7	3.5	—	2.4	(iii)
028	89R-2, 86	1436.13	1	7.1	12.4	1.8	0.7	3.7	(iii)
071	109R-3, 50	1633.31	12	7.5	10.1	6.1	—	0.2	(iii)
050	102R-1, 36	1558.33	8	4.0	1.0	3.6	—	2.4	(iv)
039	94R-1, 100	1483.21	3	2.1	1.4	2.0	—	4.8	(iv)

Notes: All analyses performed by point counting (>800 counts per section). Reported values are percentages, with groundmass the residual percentage. Petrological types are defined in the text, unit numbers refer to position in stratigraphy (see Fig. 3).

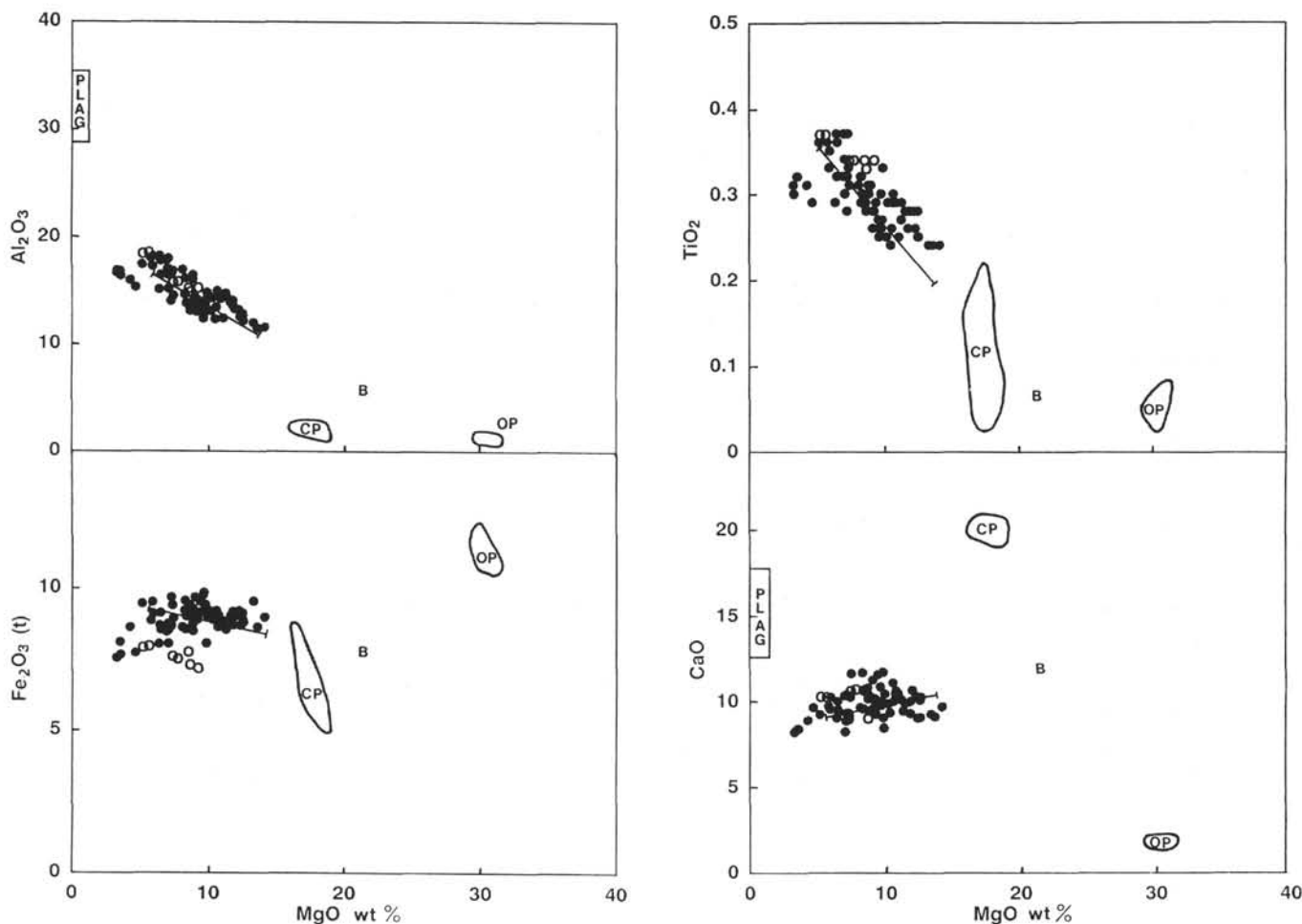


Figure 4. Major element variation with MgO for Hole 793B basement lavas. Open circles are Group A lavas, and solid circles are Group B lavas (see text). Fields are shown for the range of phenocryst compositions present in Sample 033 (analyses from Lapiere et al., this volume). OP = orthopyroxene, CP = clinopyroxene, and PLAG = plagioclase. Bulk extract (B) is a composition derived from average phenocryst analyses weighted according to their modal proportions with Sample 033. A mixing line between Group B lavas and Sample 050 (5.13 wt% MgO) represents between 2% and 55% addition of bulk extract to Sample 050.

Combining modal analyses of samples with geochemical data indicates that the proportion of individual phenocryst types changes with whole-rock chemistry. This is demonstrated in Figure 5, which shows an increase in plagioclase (as a percentage of phenocrysts present in each sample) and a decrease in orthopyroxene with declining whole-rock MgO content. As such, it is likely that whole-rock compositions are a partial function of magma evolution. However,

phenocryst content appears to be the dominant factor in whole-rock geochemical variations.

In Figure 6, trace elements are plotted against Zr as a fractionation index. The samples are divided into two groups on these plots on the basis of stratigraphic and geochemical differences. The first group (Group A) comprises the upper seven samples within Unit 1. These lava clasts have higher Zr and lower Fe contents than all underlying

Table 2. Basement geochemistry, Hole 793B.

Core, section Interval Depth (MBSF) Sample no. Unit Lithology	86R-1 128-131 1408.37 020 1 Breccia	86R-2 10-11 1409.50 021 1 Breccia	86R-2 26-30 1410.11 S-6 1 Breccia	87R-3 29-34 1419.77 024 1 Breccia	87R 22-25 1420.60 S-7 1 Breccia	88R-1 65-68 1425.50 S-8 1 Breccia	88R-1 91-95 1426.61 026 1 Breccia	89R-2 0-4 1434.44 S-9 1 Breccia	89R-2 9-12 1434.60 027 1 Breccia	89R-2 86-90 1436.13 028 1 Breccia	92R-1 20-24 1460.62 029 1 Breccia	92R-2 70-74 1465.32 030 2 Pillow	92R-2 113-117 1466.34 031 2 Pillow	92R-3 25-28 1467.79 S-10 2 Pillow	92R-3 31-35 1467.96 032 2 Pillow	92R-3 55-59 1468.50 033 2 Pillow	92R-cc 11-12 1469.51 034 2 Pillow	93R-1 63-67 1471.80 035 2 Pillow	93R-1 85-87 1472.47 S-4 2 Pillow	
Major elements (wt%)																				
SiO ₂	54.97	56.23	55.33	57.82	55.03	53.89	54.40	54.98	54.81	54.59	54.77	53.46	53.52	54.11	53.62	54.19	54.54	53.03	52.63	
TiO ₂	0.34	0.34	0.34	0.33	0.34	0.37	0.37	0.28	0.32	0.29	0.26	0.25	0.24	0.30	0.28	0.31	0.32	0.28	0.28	
Al ₂ O ₃	15.84	15.24	15.79	14.87	15.21	18.46	18.58	13.62	16.40	14.21	12.43	12.07	11.46	13.87	14.05	15.97	16.45	13.20	13.15	
Fe ₂ O ₃ *	7.50	7.16	7.59	7.29	7.74	7.91	7.95	9.09	9.08	8.84	8.64	8.74	8.93	8.44	8.84	8.70	8.64	8.96	9.16	
MnO	0.15	0.20	0.14	0.16	0.16	0.12	0.13	0.14	0.13	0.15	0.16	0.17	0.18	0.15	0.15	0.15	0.13	0.19	0.19	
MgO	7.77	9.26	7.40	8.68	8.55	5.21	5.65	9.23	6.47	10.27	12.32	12.56	14.12	8.86	9.17	8.82	7.26	11.92	12.20	
CaO	10.71	9.78	10.63	9.04	10.61	10.29	10.27	9.23	9.46	9.30	9.00	10.21	9.65	10.24	10.12	9.44	9.10	10.61	10.28	
Na ₂ O	1.65	1.48	1.73	1.66	1.81	2.23	2.24	1.78	2.15	1.75	1.57	1.78	1.45	2.30	2.25	2.03	2.31	1.59	1.57	
K ₂ O	0.93	0.43	1.12	0.82	0.66	0.92	0.91	1.09	1.28	0.56	0.46	0.58	0.18	0.88	1.03	0.42	0.89	0.20	0.26	
P ₂ O ₅	0.01	0.03	0.02	0.03	0.03	0.05	0.03	0.02	0.02	0.02	0.01	0.05	0.02	0.36	0.05	0.02	0.03	0.03	0.03	
(LOI)	2.44	3.07	1.18	4.47	1.69	1.45	2.18	1.92	2.05	1.82	2.51	1.05	1.19	1.35	1.15	1.90	2.33	2.79	1.64	
Total	99.87	100.15	100.09	100.70	100.14	99.45	100.53	99.46	100.12	99.98	99.62	99.87	99.75	99.51	99.56	100.05	99.67	100.01	99.75	
Trace elements (ppm)																				
P	31	142	93	147	152	240	108	63	103	68	61	275	140	1660	212	72	113	158	125	
Zr	42.2	43.4	42.3	41.2	41.3	44.2	44.3	27.0	33.7	27.5	25.1	24.9	24.2	27.9	29.5	31.4	30.1	26.9	26.6	
Y	8.5	11.5	10.0	10.3	10.7	16.7	12.5	9.8	10.8	8.8	7.2	18.3	9.1	20.4	21.6	9.2	12.1	11.5	10.0	
Ga	14.2	11.5	15	11.6	14.9	18.2	18.1	14.3	18.1	15.6	13.7	14.6	12.3	15	15.1	15.9	16.8	14.4	14.3	
Rb	12.9	5.2	10.6	7.4	4.9	12.4	10.8	18.2	22.1	9.9	6.4	10.9	3.2	15.3	18.4	6.0	16.1	4.4	4.5	
Sr	129	90	125	76	123	156	160	147	162	172	157	135	122	163	158	163	222	141	141	
Ba	4	0	0	15	4	10	2	13	8	11	4	6	6	19	15	7	7	1	2	
V	176	255	191	201	210	209	213	195	209	203	204	221	221	221	234	225	233	216	214	
Nb	0.5	0.3	0.3	0.6	0.4	0.4	0.2	0.4	0.3	0.0	0.3	0.0	0.4	0.4	0.1	0.8	0.2	0.0	0.1	
Ni	55	52	51	45	56	40	44	103	59	111	127	150	146	110	112	89	78	170	168	
Cr	275	282	316	236	296	126	125	566	172	347	485	748	669	399	438	204	186	561	541	
Zn	77	64	67	56	68	74	79	68	72	77	68	74	65	62	68	77	70	68	65	
Cu	18	353	17	67	66	26	24	16	22	16	23	14	14	16	16	19	48	16	18	
Nd						4.64								5.92						
Sm						1.48								1.73						
100 Mg/Mg+Fe(t)	69.5	74.0	68.2	72.4	70.9	59.2	61.0	69.1	61.1	71.9	75.8	76.0	77.7	69.8	69.5	69.1	64.9	74.5	74.6	
Al ₂ O ₃ /TiO ₂	46.6	44.8	46.4	45.1	44.7	49.9	50.2	48.6	51.3	49.0	47.8	48.3	47.8	46.2	50.2	51.5	51.4	47.1	47.0	
CaO/TiO ₂	31.5	28.8	31.3	27.4	31.2	27.8	27.8	33.0	29.6	32.1	34.6	40.8	40.2	34.1	36.1	30.5	28.4	37.9	36.7	
CaO/Al ₂ O ₃	0.68	0.64	0.67	0.61	0.70	0.56	0.55	0.68	0.58	0.65	0.72	0.85	0.84	0.74	0.72	0.59	0.55	0.80	0.78	
Ti/Zr	48	47	47	48	46	47	50	58	57	63	62	60	68	62	62	63	64	68	66	
Zr/Y	5.0	3.8	4.2	4.0	3.9	2.6	3.5	2.8	3.1	3.1	3.5	1.4	2.7	1.4	1.4	3.4	2.5	2.3	2.7	

Table 2 (continued).

Core, section Interval Depth (MBSF) Sample no. Unit Lithology	93R-1 96-100 1472.86 036 3 Breccia	93R-2 22-25 1475.28 037 3 Breccia	93R-2 27-29 1475.44 S-11 3 Breccia	93R-3 60 1476.47 038 3 Breccia	94R-1 100-105 1483.21 039 3 Breccia	94R-cc 118-126 1488.29 041 3 Breccia	96R-1 77-81 1504.07 042 4 Pillow	96R-1 81-83 1504.28 S-12 4 Pillow	96R-1 93-98 1505.16 043 4 Pillow	97R-1 80-85 1515.78 044 5 Massive	97R-1 98-102 1517.31 045 5 Massive	97R-1 124-127 1517.50 S-13 5 Massive	98R-4 63-67 1526.61 046 6 Breccia	99R-1 54-55 1530.41 S-14 7 Cpx-pill	99R-1 140-144 1534.84 048 7 Cpx-pill	100R-2 16-19 1545.10 049 8 Pillow	100R-2 28-30 1545.20 S-15 8 Pillow	102R-1 36-40 1558.33 050 8 Breccia	102R-1 128-132 1562.51 051 9 Breccia	
Major elements (wt%)																				
SiO ₂	52.73	53.51	53.41	54.37	53.71	55.15	53.14	53.48	54.36	52.64	53.17	53.19	55.03	53.02	53.66	53.96	53.50	54.05	55.26	
TiO ₂	0.28	0.37	0.37	0.32	0.37	0.36	0.29	0.29	0.36	0.28	0.29	0.28	0.32	0.27	0.26	0.33	0.35	0.36	0.34	
Al ₂ O ₃	12.76	17.90	17.71	16.07	18.17	17.70	14.15	14.46	17.97	13.97	14.88	13.83	16.91	13.50	13.34	17.19	18.13	17.37	16.37	
Fe ₂ O ₃ *	9.07	8.48	8.42	8.50	8.65	8.49	8.82	8.98	8.81	9.13	9.01	8.98	8.60	9.70	9.16	9.47	9.06	9.42	8.71	
MnO	0.19	0.15	0.15	0.16	0.14	0.16	0.18	0.16	0.13	0.20	0.19	0.20	0.15	0.16	0.17	0.13	0.13	0.11	0.15	
MgO	12.50	7.06	6.94	8.29	6.42	6.49	10.89	10.73	5.76	11.77	10.61	11.58	6.97	9.56	10.56	5.88	5.93	5.13	7.05	
CaO	10.04	10.37	10.29	9.54	9.96	9.35	10.42	10.57	9.68	9.97	10.01	9.92	8.19	10.82	9.99	9.52	10.20	9.20	8.80	
Na ₂ O	1.54	2.29	2.19	2.14	2.19	2.30	1.83	1.90	2.53	1.82	1.97	1.76	2.35	1.76	1.83	2.43	2.46	2.37	2.40	
K ₂ O	0.23	0.37	0.47	0.60	0.47	0.65	0.33	0.36	0.89	0.22	0.26	0.21	0.77	0.90	0.67	0.91	0.72	1.51	0.73	
P ₂ O ₅	0.02	0.03	0.02	0.01	0.03	0.03	0.03	0.01	0.02	0.03	0.03	0.02	0.02	0.04	0.01	0.01	0.02	0.04	0.04	
(LOI)	1.68	2.55	1.93	3.23	1.47	3.74	2.76	1.68	1.55	1.27	1.65	1.55	4.07	1.62	1.82	1.83	0.81	1.71	2.42	
Total	99.36	100.53	99.97	100.00	100.11	100.68	100.08	100.94	100.51	100.03	100.42	99.97	99.31	99.73	99.65	99.83	100.50	99.56	99.85	
Trace elements (ppm)																				
P	128	143	131	70	112	115	134	101	97	155	109	111	49	179	77	73	75	139	153	
Zr	26.3	36.3	34.6	31.4	35.8	34.6	28.8	29.1	35.2	27.8	29.5	27.6	32.4	26.6	26.1	33.3	34.4	37.5	35.9	
Y	9.7	11.9	9.8	10.3	12.2	11.1	11.3	11.1	11.6	13.0	10.0	8.8	8.5	11.5	9.3	10.1	10.6	13.6	12.5	
Ga	13.8	16.4	15	17.5	16.3	14.9	15.1	18.8	14.4	14.9	13.5	15.9	15.6	14.5	17.3	17.4	18.3	15.9		
Rb	4.4	4.8	3.9	2.8	6.8	6.6	5.8	7.2	13.4	4.4	3.2	3.5	9.6	17.2	12.8	16.4	12.0	27.1	7.2	
Sr	141	190	184	154	189	164	149	152	193	149	151	140	176	140	132	187	197	184	152	
Ba	2	0	13	8	5	5	0	5	9	1	0	3	23	11	12	0	4	0	1	
V	216	259	260	214	252	231	231	230	222	221	237	211	215	256	229	233	247	244	254	
Nb	0.5	0.4	0.5	0.2	0.4	0.1	0.1	0.6	0.0	0.1	0.5	0.4	0.1	0.6	0.5	0.5	0.4	0.4	0.4	
Ni	161	56	55	78	46	42	138	140	45	127	107	123	39	122	137	59	48	51	46	
Cr	491	174	144	260	74	73	569	544	70	432	390	488	39	596	491	62	87	126	162	
Zn	66	70	88	71	72	67	83	79	76	67	66	64	69	75	79	85	87	75	65	
Cu	18	72	76	19	25	45	18	19	19	22	16	24	129	15	34	21	19	18	164	
Nd								3.63				2.46		3.69						
Sm								1.20				0.84		1.21						
100 Mg/Mg+Fe(t)	75.2	64.7	64.5	68.2	62.0	62.7	73.1	72.5	59.0	73.9	72.2	73.9	64.1	68.4	71.7	57.7	59.0	54.5	64.0	
Al ₂ O ₃ /TiO ₂	45.6	48.4	47.9	50.2	49.1	49.2	48.8	49.9	49.9	49.9	51.3	49.4	52.8	50.0	51.3	52.1	51.8	48.3	48.1	
CaO/TiO ₂	35.9	28.0	27.8	29.8	26.9	26.0	35.9	36.4	26.9	35.6	34.5	35.4	25.6	40.1	38.4	28.8	29.1	25.6	25.9	
CaO/Al ₂ O ₃	0.79	0.58	0.58	0.59	0.55	0.53	0.74	0.73	0.54	0.71	0.67	0.72	0.48	0.80	0.75	0.55	0.56	0.53	0.54	
Ti/Zr	69	64	64	63	62	60	64	60	61	62	63	61	59	63	65	61	60	59	58	
Zr/Y	2.7	3.1	2.5	3.0	2.9	3.1	2.5	2.6	3.0	2.1	3.0	3.1	3.8	2.3	2.8	3.3	3.2	2.8	2.9	

Table 2 (continued).

Core, section Interval	103R-1 123-127	104R-1 65-70	104R-1 140-145	104R-2 49-54	104R-2 69-75	104R-3 95-100	105R-1 1-6	105R-1 127-131	105R-3 106-110	106R-2 28-33	107R-1 10-14	107R-1 17-20	107R-3 10-16	108R-1 55-60	108R-2 0-7	109R-2 127-132	109R-3 50-55	109R-3 50-55	110R-1 1-3	
Depth (MBSF)	1569.78	1577.11	1578.49	1579.56	1579.92	1583.11	1585.61	1588.38	1594.47	1605.43	1605.01	1605.10	1610.26	1615.96	1618.64	1631.40	1633.31	1633.31	1633.83	
Sample no.	052	053	054	S-16	055	056	058	S-17	063	062	064	S-18	065	068	069	070	071 (a)	071 (b)	S-19	
Unit	9	10	10	10	10	10	11	11	11	11	11	11	12	12	12	12	12	12	13	
Lithology	Breccia	Massive	Massive	Massive	Massive	Massive	Pillow	Pillow	Pillow	Pillow	Pillow	Pillow	Breccia	Breccia	Breccia	Breccia	Breccia	Breccia	Breccia	massive
Major elements (wt%)																				
SiO ₂	53.95	52.80	52.88	53.18	53.37	53.69	55.20	56.04	54.41	54.01	57.26	53.51	53.34	53.28	52.53	53.07	56.13	54.28	54.56	
TiO ₂	0.37	0.30	0.31	0.32	0.31	0.29	0.30	0.28	0.29	0.29	0.29	0.33	0.33	0.27	0.30	0.29	0.27	0.26	0.25	
Al ₂ O ₃	16.83	13.68	14.28	14.55	14.45	13.54	13.74	13.03	13.46	14.57	15.26	16.78	14.73	14.64	14.70	14.40	14.04	13.50	13.02	
Fe ₂ O ₃ *	9.63	9.36	9.63	9.17	8.90	9.48	8.96	9.09	9.35	9.51	7.68	9.35	8.97	8.49	8.59	8.77	8.01	8.66	9.14	
MnO	0.14	0.16	0.17	0.16	0.14	0.17	0.17	0.17	0.17	0.17	0.13	0.14	0.17	0.16	0.16	0.17	0.14	0.17	0.15	
MgO	7.27	9.76	8.99	8.23	7.41	9.37	8.37	8.66	8.61	8.28	4.64	7.34	9.88	11.26	10.67	11.30	9.83	11.79	10.15	
CaO	8.90	11.66	11.22	11.62	11.57	11.52	10.54	10.11	10.75	10.63	9.61	10.20	10.39	9.42	10.42	9.95	8.41	9.25	9.83	
Na ₂ O	2.31	1.78	2.03	2.17	2.27	1.98	2.24	2.04	1.77	2.15	2.74	2.26	1.81	1.89	1.87	1.86	2.05	1.73	2.29	
K ₂ O	0.55	0.28	0.29	0.51	0.91	0.20	0.46	0.46	0.64	0.24	1.39	0.50	0.32	0.26	0.26	0.22	0.58	0.34	0.69	
P ₂ O ₅	0.02	0.02	0.03	0.06	0.13	0.03	0.03	0.03	0.03	0.03	0.51	0.02	0.03	0.02	0.04	0.02	0.03	0.02	0.04	
(LOI)	1.24	1.30	1.42	0.83	1.69	2.14	2.60	2.27	2.31	1.32	0.48	1.42	1.31	1.99	1.65	1.33	1.96	1.59	0.77	
Total	99.97	99.80	99.83	99.97	99.46	100.27	100.01	99.91	99.48	99.88	99.51	100.43	99.97	99.69	99.54	100.05	99.49	100.00	100.12	
Trace elements (ppm)																				
P	81	107	163	292	754	145	150	125	142	208	2350	77	118	96	181	114	101	74	201	
Zr	36.8	32.6	32.1	33.5	31.2	30.1	33.0	31.2	31.5	34.7	34.0	34.7	33.3	30.7	28.1	28.1	31.0	29.7	25.1	
Y	10.1	10.1	11.7	15.4	21.7	9.8	10.6	10.4	10.0	12.1	50.9	9.9	11.2	9.9	11.6	10.0	9.8	10.1	13.0	
Ga	18	15.6	15.2	16.3	16.8	14.3	15.2	12.7	15.7	15.5	15.9	17.2	14.6	14.8	15.8	16.4	13.1	13	13.5	
Rb	8.1	4.7	4.7	9.6	16.9	2.5	5.0	5.8	10.0	4.3	22.5	8.7	6.2	4.2	5.0	5.0	9.7	4.8	11.5	
Sr	170	161	174	178	201	234	145	129	157	180	197	183	150	153	147	145	153	129	147	
Ba	0	4	3	7	14	12	8	6	10	10	38	7	0	4	2	1	28	0	20	
V	235	253	259	259	264	244	239	231	225	245	221	237	235	205	233	218	189	200	249	
Nb	0.6	0.2	0.3	0.5	0.1	0.5	0.4	0.5	0.0	0.6	0.0	0.4	0.6	0.0	0.0	0.2	0.1	0.0	0.5	
Ni	42	48	45	49	49	44	34	38	45	36	27	37	106	134	124	123	123	132	124	
Cr	63	244	240	270	278	235	189	221	280	159	139	162	320	400	351	345	449	490	647	
Zn	75	83	81	76	77	66	66	64	72	71	58	86	77	65	70	68	59	64	65	
Cu	20	19	29	18	57	53	139	72	91	23	98	169	16	55	20	43	68	120	102	
Nd				5.61				2.77											3.46	
Sm				1.78				0.97											1.06	
100 Mg/Mg+Fe(t)	62.4	69.7	67.3	66.4	64.7	68.5	67.3	67.7	67.0	65.7	57.1	63.3	70.8	74.5	73.2	73.9	73.0	75.0	71.0	
Al ₂ O ₃ /TiO ₂	45.5	45.6	46.1	45.5	46.6	46.7	45.8	46.5	46.4	50.2	52.6	50.8	44.6	54.2	49.0	49.7	52.0	51.9	52.1	
CaO/TiO ₂	24.1	38.9	36.2	36.3	37.3	39.7	35.1	36.1	37.1	36.7	33.1	30.9	31.5	34.9	34.7	34.3	31.1	35.6	39.3	
CaO/Al ₂ O ₃	0.53	0.85	0.79	0.80	0.80	0.85	0.77	0.78	0.80	0.73	0.63	0.61	0.71	0.64	0.71	0.69	0.60	0.69	0.75	
Ti/Zr	59	67	65	60	68	65	60	57	62	60	54	58	64	58	71	70	50	56	62	
Zr/Y	3.6	3.2	2.7	2.2	1.4	3.1	3.1	3.0	3.2	2.9	0.7	3.5	3.0	3.1	2.4	2.8	3.2	2.9	1.9	

Table 2 (continued).

Core, section Interval	110R-1 7-12	110R-2 115-125	110R-2 115-125	110R-3 78-83	110R-4 57-62	110R-5 128-132	111R-1 110-115	111R-2 32-37	111R-2 111-116	112R-1 59-63	112R-1 63-68	112R-1 93-97	112R-2 57-62	112R-2 140-149	113R-2 13-17	113R-2 133-138	113R-3 130-135	113R-3 137-141	113R-4 35-41
Depth (MBSF)	1633.96	1637.86	1637.86	1638.97	1640.48	1643.20	1645.89	1648.53	1650.61	1654.72	1655.20	1656.33	1661.38	1662.50	1666.50	1669.35	1670.23	1671.40	1672.30
Sample no.	072	073(a)	073(b)	075	074	076	079	077	078	S-20	080	081	083	084	085	086	087	S-21	088
Unit	13	13	13	13	13	14	14	14	14	14	14	14	14	15	15	15	16	16	16
Lithology	Massive	Massive	Massive	Massive	Massive	Massive	Massive	Massive	Massive	Massive	Massive	Massive	Massive	Massive	Breccia	Breccia	Massive	Massive	Massive
Major elements (wt%)																			
SiO ₂	53.99	55.44	55.12	54.41	53.72	56.71	54.82	52.93	54.30	55.51	56.77	55.53	53.75	57.92	52.81	52.97	57.83	59.29	58.84
TiO ₂	0.25	0.26	0.25	0.26	0.24	0.31	0.26	0.24	0.24	0.30	0.29	0.28	0.25	0.32	0.30	0.31	0.32	0.31	0.30
Al ₂ O ₃	12.33	12.93	12.29	12.66	12.24	15.92	13.17	11.91	11.37	15.08	15.04	13.96	12.58	16.32	16.36	16.86	16.74	16.61	16.83
Fe ₂ O ₃ *	8.80	8.94	9.79	9.18	8.94	8.59	9.12	9.49	8.59	8.00	7.99	8.61	8.84	7.62	9.23	8.57	8.07	7.51	7.51
MnO	0.15	0.14	0.15	0.15	0.16	0.11	0.13	0.14	0.16	0.12	0.12	0.12	0.16	0.10	0.15	0.13	0.10	0.09	0.09
MgO	11.08	9.14	9.62	9.64	10.49	4.24	9.78	13.31	13.61	7.06	6.35	7.23	12.51	3.55	8.84	8.07	3.51	3.24	3.28
CaO	10.09	9.63	9.74	9.99	11.04	8.86	9.01	9.22	9.07	9.28	8.99	9.27	9.03	8.36	9.37	9.61	8.37	8.16	8.22
Na ₂ O	2.15	2.42	2.36	2.32	2.22	3.11	2.42	1.76	1.91	2.71	2.80	2.52	2.04	3.09	2.15	2.47	3.10	3.03	3.14
K ₂ O	0.60	0.77	0.88	0.75	0.77	1.48	0.96	0.60	0.33	1.19	1.37	1.51	0.35	1.69	0.31	0.50	1.85	1.69	1.72
P ₂ O ₅	0.03	0.04	0.04	0.04	0.04	0.09	0.05	0.05	0.03	0.69	0.52	0.66	0.11	0.35	0.02	0.01	0.06	0.06	0.06
(LOI)	1.34	1.19	1.49	1.87	1.81	1.12	1.68	2.35	1.60	0.90	0.86	1.48	1.46	1.41	1.91	1.68	0.83	0.64	1.04
Total	99.47	99.71	100.24	99.40	99.86	99.42	99.72	99.65	99.61	99.94	100.24	99.69	99.62	99.32	99.54	99.50	99.95	99.99	99.99
Trace elements (ppm)																			
P	195	205	194	191	185	434	248	292	160	3589	2815	3422	637	1829	94	80	269	279	254
Zr	24.1	25.9	24.4	24.5	23.2	30.8	25.4	23.0	23.5	29.7	30.5	27.9	25.7	33.4	33.7	33.9	35.5	34.4	33.4
Y	12.3	12.8	12.5	12.4	11.3	20.7	11.0	15.4	8.9	18.5	21.3	24.3	11.7	49.7	9.6	8.5	21.9	21.6	21.9
Ga	13.7	14.5	13.7	13.8	13.9	16.4	14.6	13.1	12.2	14.4	14.9	14.2	13.1	16.3	16.3	16.8	19.1	18.5	17.1
Rb	10.1	15.2	17.8	12.7	13.2	33.0	20.6	13.3	7.4	25.3	31.7	36.9	7.0	33.5	5.4	8.9	35.4	31.5	31.3
Sr	142	151	136	143	139	191	152	131	130	187	183	172	143	197	184	182	197	196	195
Ba	5	14	26	18	21	13	20	0	19	22	25	19	16	21	8	8	32	25	17
V	219	221	215	214	248	221	202	188	209	221	216	196	215	219	247	249	237	227	220
Nb	0.0	0.0	0.3	0.2	0.3	0.0	0.2	0.6	0.4	0.3	0.0	0.3	0.5	0.0	0.2	0.0	0.2	0.2	0.3
Ni	139	90	114	100	112	40	126	146	158	83	71	89	143	36	81	87	28	23	21
Cr	637	453	737	563	606	92	493	565	670	239	222	366	536	56	219	238	41	40	33
Zn	64	59	64	57	57	61	65	68	65	58	53	55	70	51	74	75	58	51	51
Cu	28	36	45	130	44	112	14	6	54	19	22	25	12	21	142	361	15	38	25
Nd										3.28								7.36	
Sm										1.04								2.32	
100 Mg/Mg+Fe(t)	73.5	69.2	68.4	69.8	72.1	52.1	70.2	75.5	77.7	66.0	63.6	64.9	75.7	50.6	67.8	67.5	48.9	48.7	49.0
Al ₂ O ₃ /TiO ₂	49.3	49.7	49.2	48.7	51.0	51.4	50.7	49.6	47.4	50.3	51.9	49.9	50.3	51.0	54.5	54.4	52.3	53.6	56.1
CaO/TiO ₂	40.4	37.0	39.0	38.4	46.0	28.6	34.7	38.4	37.8	30.9	31.0	33.1	36.1	26.1	31.2	31.0	26.2	26.3	27.4
CaO/Al ₂ O ₃	0.82	0.74	0.79	0.79	0.90	0.56	0.68	0.77	0.80	0.62	0.60	0.66	0.72	0.51	0.57	0.57	0.50	0.49	0.49
Ti/Zr	65	63	62	58	70	58	65	67	66	61	59	59	63	57	60	63	56	55	54
Zr/Y	2.0	2.0	2.0	2.0	2.1	1.5	2.3	1.5	2.6	1.6	1.4	1.1	2.2	0.7	3.5	4.0	1.6	1.6	1.5

Table 3. Least squares mixing calculations, Hole 793B basement.

	Model 1 Sample 030 to sample 033 (12.58 to 8.82 wt% MgO)				Model 2 Sample 030 to sample 050 (12.58 to 5.16 wt % MgO)				Model 3 Sample 033 to sample 050 (8.82 to 5.16 wt % MgO)			
	Parent analysis	Daughter analysis	Daughter calculated	Residual	Parent analysis	Daughter analysis	Daughter calculated	Residual	Parent analysis	Daughter analysis	Daughter calculated	Residual
SiO ₂	53.53	54.16	53.28	0.88	53.53	54.29	53.57	0.72	54.16	54.29	54.83	-0.54
TiO ₂	0.25	0.31	0.31	0.00	0.25	0.36	0.42	-0.06	0.31	0.36	0.42	-0.06
Al ₂ O ₃	12.09	15.96	15.83	0.13	12.09	17.45	17.38	0.07	15.96	17.45	17.56	-0.11
Fe ₂ O ₃	8.75	8.70	8.86	-0.16	8.75	9.46	9.64	-0.18	8.70	9.46	9.45	0.02
MnO	0.17	0.15	0.17	-0.02	0.17	0.11	0.18	-0.07	0.15	0.11	0.16	-0.05
MgO	12.58	8.82	8.85	-0.03	12.58	5.15	5.28	-0.13	8.82	5.15	5.16	0.00
CaO	10.22	9.44	9.46	-0.03	10.22	9.24	9.32	-0.08	9.44	9.24	9.27	-0.03
Na ₂ O	1.78	2.03	2.38	-0.35	1.78	2.38	3.04	-0.66	2.03	2.38	2.57	-0.18
K ₂ O	0.58	0.42	0.79	-0.37	0.58	1.52	1.07	0.44	0.42	1.52	0.57	0.95
P ₂ O ₅	0.05	0.02	0.07	-0.05	0.05	0.04	0.09	-0.05	0.02	0.04	0.03	0.01
	Sum R squared			1.08	Sum R squared			1.22	Sum R squared			1.25
	26.5% crystallization as:		cpx : opx 58 : 42		47.3% crystallization as:		cpx : opx : plag 45 : 40 : 15		28.6% crystallization as:		cpx : opx : plag 17 : 49 : 34	
	Sample 030 contains 41.6% phenocrysts as:		cpx : opx : plag 58 : 41 : 0.7		Sample 033 contains 16.7% phenocrysts as:		cpx : opx : plag 37 : 41 : 22		Sample 050 contains 8.8% phenocrysts as:		cpx : opx : plag 46 : 11 : 43	

Notes: Modal proportions calculated on a vesicle-free basis. Mineral compositions taken as averages of phenocryst analyses from sample 033 (Lapierre et al., this volume).

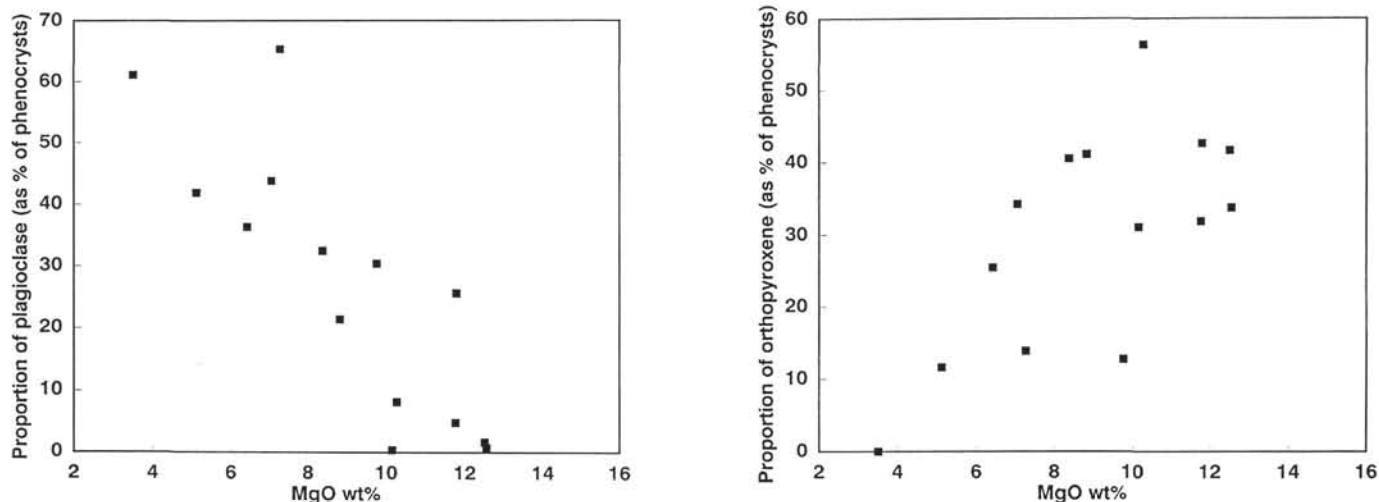


Figure 5. MgO contents of Hole 793B basement plotted vs. the proportion of plagioclase and orthopyroxene expressed as a percentage of total phenocrysts. Modal analyses are given in Table 1.

lavas of Group B (see also Fig. 4). Clinopyroxene analyses from Group A lavas reflect the whole-rock compositions in having appropriately lower Fe/Mg ratios and total Fe contents (see Lapiere et al., this volume). Both groups show positive correlations between Zr and Ti, Ga, Sr, and Al_2O_3 , with inter-element ratios remaining roughly constant. Ni and Cr correlate negatively with Zr, reflecting the removal or addition of pyroxenes.

Aspects of Trace Element Enrichment

Relationships between Zr and certain other trace elements are not as easily explained. On Figure 6, P and Y show no correlation with Zr and Sm + Nd a very weak one. Yttrium varies by a factor of 5 and P by a factor of 30 in samples ranging from 25 to 35 ppm Zr. Similar, though less pronounced discrepancies, are noted in the combined Nd and Sm against Zr plot. Figure 7 demonstrates the anomalous behavior of certain trace elements. On this plot, concentrations of a low-MgO (anomalous) sample (S-21: 126-793B-113R-3, 137–141 cm) are normalized to a primitive high-MgO sample (S-13: 126-793B-98R-3, 124–127 cm). Also shown for comparison on Figure 7 are predicted trace element concentrations after removal of 30% and 80% of observed phenocrysts in S-13. Of the trace elements, only Sr, Ti, Zr, and Ga are close to predicted concentrations after 30% crystallization. Levels of P, Y, Nd, Sm, and the low-field-strength elements (LFSE) are all significantly higher, requiring in excess of 70% crystallization to generate the observed concentrations. REE patterns from two basement samples (Table 4 and Fig. 8) show nonparallel profiles, suggesting a process other than crystallization relates lavas within the sequence.

As elements such as P, Y, and the REE are normally considered to be immobile during low-temperature hydrothermal alteration (e.g., Saunders et al., 1980), the possibility of a primary magmatic origin for the trace element peculiarities must be examined. Because lower MgO samples tend to be the most affected by P and Y enrichment, it is possible that an assimilation/crystallization or magma mixing process may be responsible. To test this hypothesis, a single massive flow containing a range of phenocryst abundances and MgO contents was examined. Subunit 14a (Fig. 3) is a suitable flow with recognizable upper and lower contacts and good recovery. Six whole-rock samples were analyzed from this flow with a view to examining its internal chemical variations.

Geochemical profiles throughout the Subunit 14a flow are shown in Figure 9. Phenocrysts tend to be concentrated in the center of the unit, reflecting a flowage differentiation during extrusion. Variations

within major element, Zr, Ga, Cr, Ni, Sr, and V profiles can be explained by dilution of the erupted liquid by the observed phenocryst abundances. However, the profiles for P, Y, K_2O , and Rb do not fit a simple dilution model. K_2O and Rb are enriched by factors of 3–4 between the low- and high-MgO samples, far greater than the enrichment factors of 1.3–1.5 for Sr, Ti, Zr, and Ga. Phosphorus and yttrium are also over-enriched in the lower MgO samples, however, in contrast to Rb and K_2O , concentrations of these elements are greatest in the two samples from the base of the flow. The enrichment in P between the center and the base of the flow is by factors of 18–22. Similar P and Y anomalies were found throughout the section but are only recognized within massive and pillowed flows and were absent in samples taken from breccia units (see P-Zr and Y-Zr plots, Fig. 6).

In light of the known mobility of elements such as K and Rb during alteration, enrichment in the low-MgO sections of Subunit 14a can be explained by hydrothermal redistribution of these elements within the flow. On a broad scale, samples with high K_2O also tend to have greater concentrations of P and Y. However, the over-enrichment of P at the base of Subunit 14a suggests that another event or process may have disturbed the original igneous concentrations. Clearly, assimilation of host lithologies, either before or after eruption, is unlikely to produce such extreme enrichment within a single flow.

The most likely explanation for anomalous P, Y, and the rare-earth element (REE) concentrations relative to HFS elements is a low-temperature hydrothermal alteration process. Bienvenu et al. (1990) have described the systematic removal of REE, Y, and P and retention of Zr and Ti during alteration of mid-ocean ridge basalt (MORB) glasses to smectite. In the case of these oceanic lavas, the trivalent elements and P were removed from the system during fluid (seawater) interaction. In contrast, Zr and Ti remained in the glass/smectite system because of their high ionic potential and hydrolytic properties. Similar smectitization took place in Hole 793B lavas during hydrothermal circulation within the basement after eruption. However, the heterogeneous nature of the Hole 793B basement (namely, the intercalations of breccias and flows) has clearly affected fluid flow and element redistribution. Breccia units, which lack the anomalous P, Y, and REE values (Fig. 6), may act as permeable pathways for the efficient removal of fluids from the system without deposition of the solute. In contrast, massive and pillowed flows are less permeable and simply redistribute the mobilized elements internally. This has produced regions within flows where element leaching has occurred, and other areas (notably the base of Subunit 14a) where precipitation is dominant. The behavior of Mg, Fe, and Al with the sequence

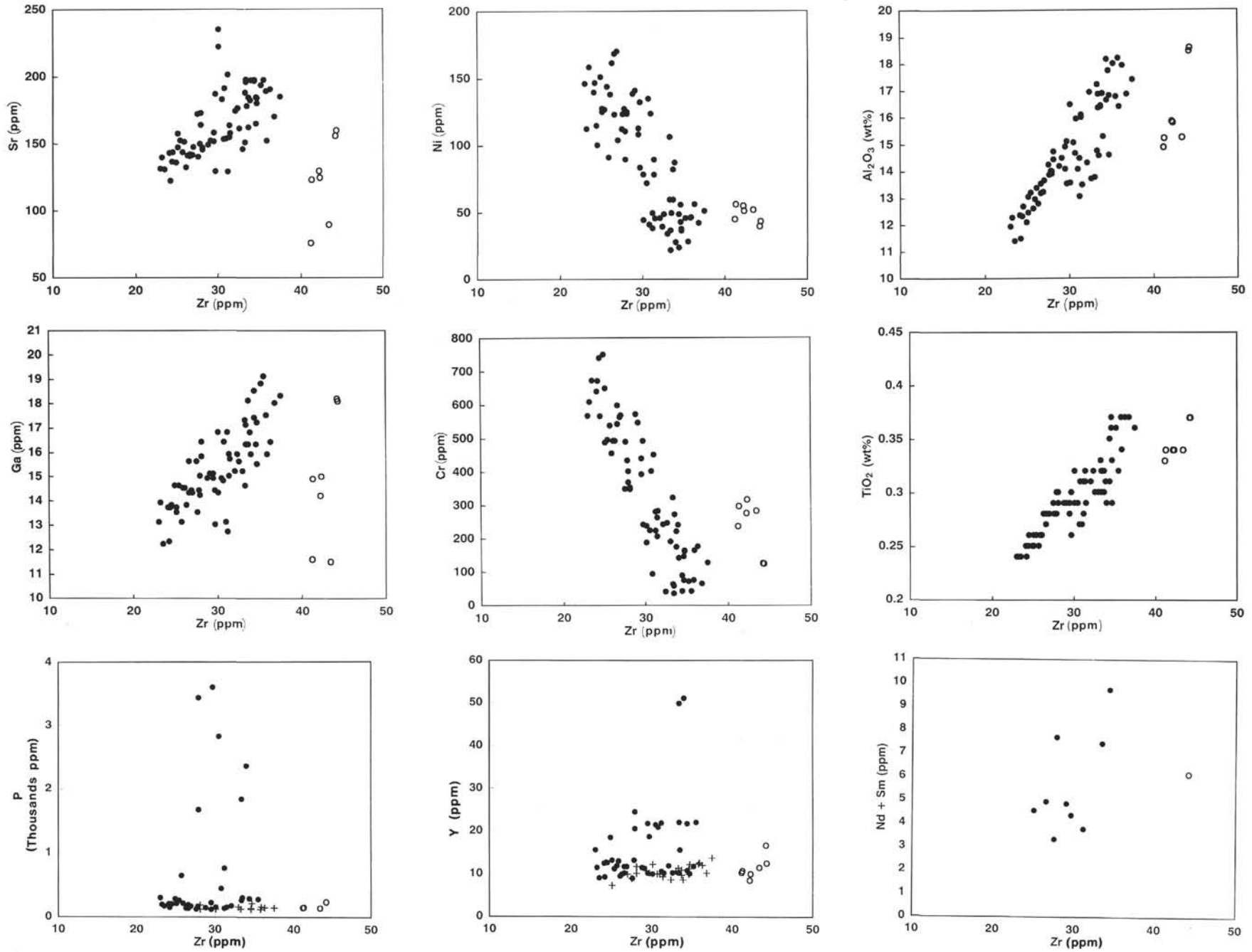


Figure 6. Trace elements (ppm) and TiO₂ and Al₂O₃ (wt%) plotted vs. Zr (ppm) for Hole 793B basement. Open circles = Group A lavas, and filled circles = Group B lavas.

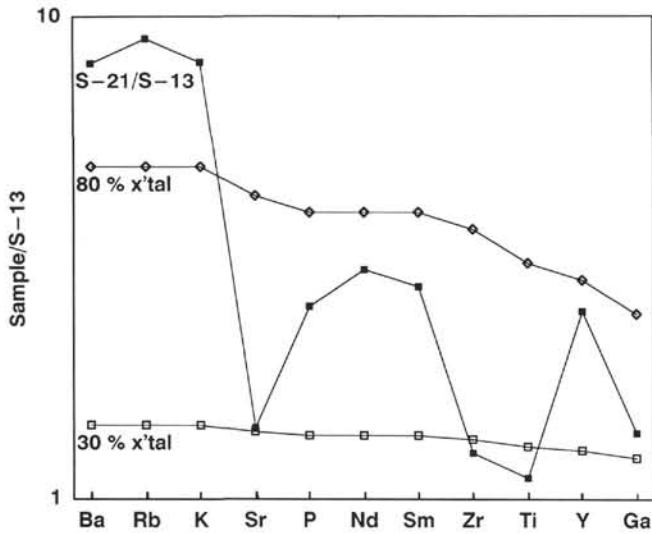


Figure 7. Trace element concentration of Sample S-21 (3.24 wt% MgO) normalized to Sample S-13 (11.58 wt% MgO). Also shown are predicted profiles for magmas generated by 30% and 80% crystallization (x' tal) of Sample S-13. Crystallization modeled using distribution coefficients from Henderson (1982) and phase proportions $\text{cpx:opx:plag} = 5:4:1$.

appears to be commensurate with crystal fractionation/accumulation processes. This can be ascribed to the locking of these elements in the saponite/celadonite/illite alteration products that replace the interstitial glass (for details of clay chemistry, see Lapiere et al., this volume).

Interestingly, Sr, which is normally considered to be mobile, shows a variation within the sequence commensurate with primary igneous fractionation. This Sr behavior can be explained by its location within the whole-rock system. All lavas within Hole 793B have abundant plagioclase laths and microlites in their groundmass. Strontium would behave incompatibly during ol-opx-cpx crystallization, concentrating in the liquid with Zr, Ti, P, and the REE. However, during final solidification, Sr would partition strongly into the plagioclase microphenocrysts, leaving the incompatible elements in the interstitial glass. During alteration the glass underwent smecti-

Table 4. Rare earth element analyses, Hole 793B basement.

Sample	S-12	S-20	Detection limits
Core, section	96R-1	112R-1	
Interval (cm)	81-83 cm	59-63 cm	
Unit	4	14a	
La	1.89	—	0.1
Ce	4.95	5.51	0.1
Nd	3.63	3.28	0.02
Sm	1.20	1.04	0.015
Eu	0.42	0.39	0.015
Gd	1.57	1.52	0.2
Dy	1.54	1.78	0.02
Er	0.99	1.33	0.02
Yb	1.03	1.52	0.02
Lu	0.18	0.28	0.015

All concentrations in parts per million. Analysis by isotope dilution mass spectrometry using the technique described by Croudace and Marshall (1991), at the Department of Geology, University of Southampton, U.K.

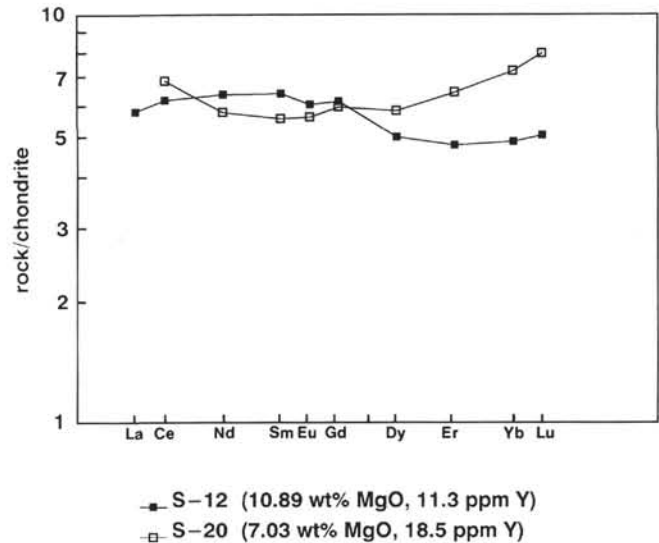


Figure 8. Chondrite-normalized, rare-earth element (REE) profiles for Hole 793B basement lavas. Chondrite values from Kay and Gast (1973).

tization (and possibly illitization) causing partitioning of REE, P, and Y into circulating fluids and leaving hydrolyzed Ti and Zr in or around clays, and the Sr locked in plagioclase. Sr isotope results (see below) clearly indicate that a minor isotopic exchange between rock and seawater-based fluids has taken place. However, strontium concentrations remain close to the original magmatic abundances.

Forearc Diabase Intrusive

A diabase sill intruding 14-Ma sediments was encountered at a depth of 586 m in Hole 793B. Petrographically, the intrusion contains phenocrysts of clinopyroxene, orthopyroxene, and plagioclase and pseudomorphs of olivine. Titanomagnetite was found throughout the intrusion, but it is restricted to the groundmass. Further details of the internal structure and petrography are given in Taylor, Fujioka, et al. (1990) and of the mineral chemistry in Lapiere et al. (this volume).

Major and trace element geochemistry of the intrusion (Table 5) indicates a tholeiitic affinity. Trace element ratios such as Ti/Zr (100), Zr/Y (2), and Ti/V (12) of the diabase are similar to those of the active Izu arc volcanoes of Tori Shima and Sumisu Jima (Shipboard Scientific Party, 1990). A tholeiitic basalt clast derived from the active arc was found in early to middle Miocene sediments (610 mbsf) of Hole 793B. This clast has a similar composition (Sample 012, Table 5) to the diabase, supporting the association of the sill with the active arc.

Laterally extensive seismic reflectors were found across the forearc region (B. Taylor, pers. comm., 1990), which may represent intrusions such as the diabase. In light of these reflectors and the diabase chemistry, it is likely that the intrusion represents a continuation of arc magmatism into the forearc region, or the lateral injection of magmas from the active arc into forearc sediments.

SITE 792

The Oligocene Arc

Multichannel seismic profiles across the Izu-Bonin arc have shown the presence of a series of basement promontories, spaced about every 60-100 km, and located 30-40 km east (trenchward) of the active arc chain (Taylor et al., 1990). These frontal-arc basement highs were recognized by Honza and Tamaki (1985), who named them the Shinkurose Ridge. Initial interpretations designated the ridge as the remnants of an earlier arc-volcano chain, now buried by sediments during the formation of the forearc basin. Hole 792E drilled through

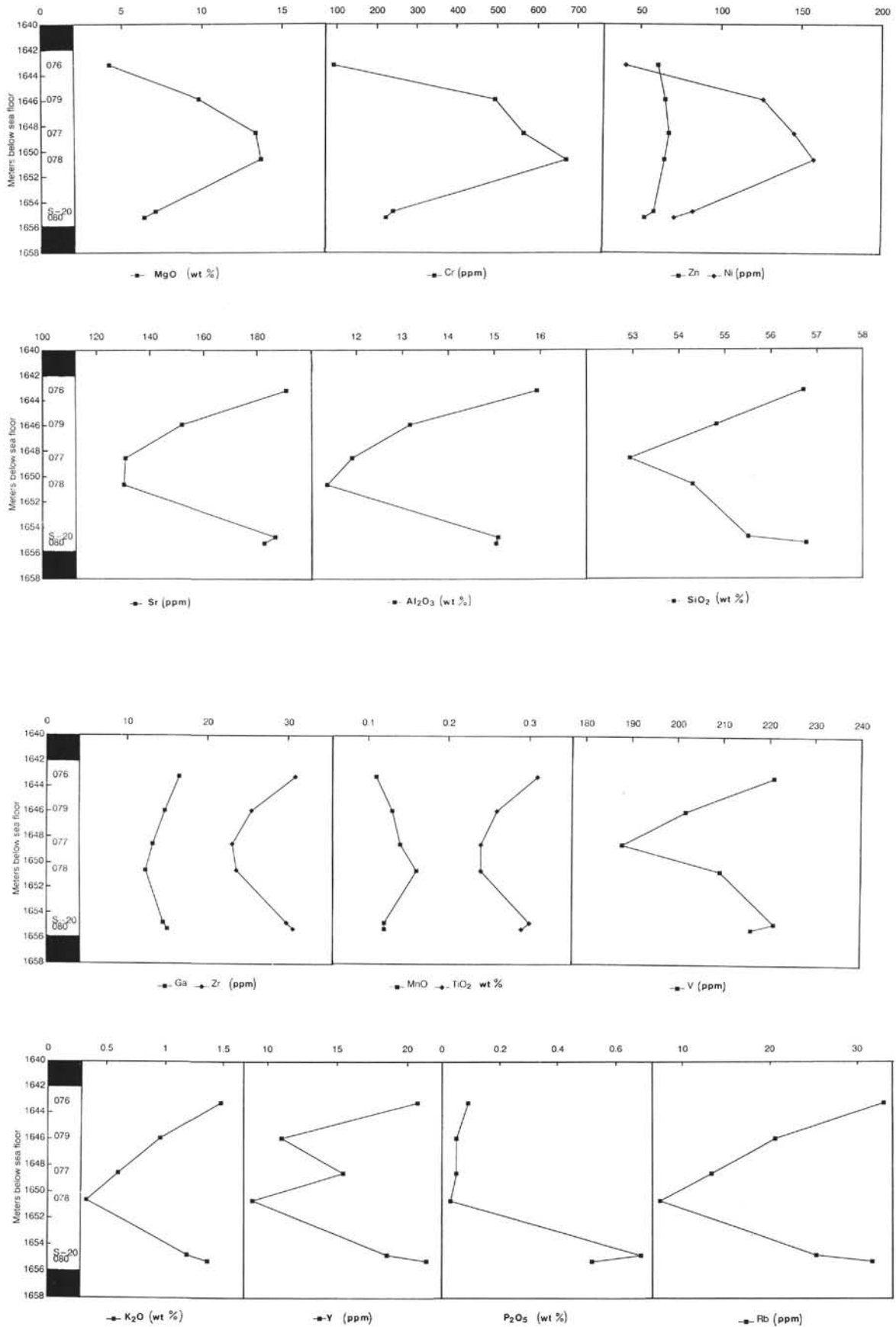


Figure 9. Geochemical profiles through Subunit 14a, Hole 793B basement. Sample numbers used are shown on the left.

the marginal sediments of the basin and penetrated 82 m of basement volcanics on a basement high at 32° 24' N (Fig. 2). The sediments overlying basement were constrained biostratigraphically and magnetostratigraphically as late Oligocene (30–32 Ma), whereas basement volcanics were radiometrically dated as 33 Ma. Details of the materials used, analytical procedures, and interpretation of the radiometric ages are given in Taylor and Mitchell (this volume).

Sediments in the 10 m directly overlying basement are hydrothermally altered volcanoclastic sandstones and conglomerates with clasts of andesite, claystone, and extremely fresh amphibole crystals. The matrix is dominantly blue-grey smectite, replacing original vitric detritus. These sediments suggest that post-eruptive hydrothermal circulation above the basement was concentrated in a restricted horizon. Alteration was probably induced by low-temperature (<200°C) porewater circulation, in a similar fashion to the vitric-sediment/porewater interaction envisaged for the overlying sediments by Egeberg (1990). Initial studies of the basement lavas indicate a similarly low-temperature alteration with partial replacement of some original phases by smectite, zeolite, and carbonate.

Volcanic Stratigraphy and Eruptive Setting

Basement volcanics in Hole 792E are subdivided into five major units (Fig. 10). The dominant lithology is massive flows of two-pyroxene andesite (estimated at 5–10 m thickness Taylor, Fujioka, et al., 1990) with subordinate dacite, rhyolite, and basaltic andesite. These are intercalated with hyaloclastite breccia layers containing similar mineral species and proportions to the massive flows, but they have matrices of smectitized vitric shards. A single heterolithic volcanogenic breccia is found in the volcanic sequence (Unit 4). This contains subrounded clasts similar to the surrounding flows and a single clast of prehnite-chlorite-bearing meta-basalt. Detailed descriptions of the lithologic units are given in Taylor, Fujioka, et al. (1990).

The combination of hyaloclastitic layers and a heterolithic sedimentary horizon suggests that the volcanics were the products of submarine eruptions. This is consistent with a number of scenarios, any or all of which are plausible: (1) that the volcanic edifice was never emergent above sea level, either because of arc-rifting during construction, or cessation of arc volcanoes, (2) that Site 792 was located on the submerged flank of an arc volcano, and/or (3) that the original volcano has been denuded to its submarine base by subsequent erosion.

Petrography

Basement volcanics within Hole 792E are petrographically similar to many calc-alkaline lavas in the active Japan Arc. Plagioclase is an abundant and ubiquitous phenocryst (20–30 modal%) throughout the sequence; it is found associated with two pyroxenes: titanomagnetite and sometimes quartz (Plate 2). The crystallization sequence of plag + oxide → opx + cpx → quartz is also typically calc-alkaline. Modal analyses of the lavas are given in Table 6. Quartz is found in all lavas from the lowest 55 m of the stratigraphy (Fig. 10), regardless of their whole-rock SiO₂ contents. A brief outline of the mineralogy is given below; a more detailed analysis is given in Lapiere et al. (this volume).

Magnetite

Subhedral grains 0.3–2 mm in size, existing as phenocrysts in the groundmass and as inclusions within clino- and orthopyroxene.

Plagioclase

Euhedral to subhedral fresh phenocrysts 0.5–5 mm in size. Strong oscillatory zoning is common, with compositions ranging from An₆₄ to An₈₄. Fluid and glass inclusions are abundant, but are restricted to a growth zone between core and rim.

Clinopyroxene

Euhedral to subhedral unaltered phenocrysts 0.3–3 mm in size. Zoning is prevalent in most crystals with compositions En₄₉:Wo₄₀:Fs₁₁–En₃₈:Wo₄₃:Fs₁₉. Magnetite and glass are found as inclusions in the larger phenocrysts.

Orthopyroxene

Subhedral phenocrysts 0.3–3 mm in size are found throughout the sequence; however, with the exception of the uppermost 15 m of the stratigraphy, are pseudomorphed by clays. The orthopyroxene in the upper flows of Unit 1 have fresh cores mantled by alteration zones comprising a mixture of smectite and cristobalite.

Quartz

Occurs as subrounded to rounded euhedral grains < 0.1–0.7 mm in size.

Geochemistry

We analyzed a series of 26 basement volcanics from Hole 792E to constrain the geochemical characteristics of the Oligocene Izu-Bonin arc. Major and trace element data are presented in Table 7. The major element data reveal a diverse compositional range within the 82 m of basement drilled. Samples range from basaltic andesites, through andesites and dacites, to rhyolite (about 53–72 wt% SiO₂ and 1–7 wt% MgO). Evolutionary trends within the major element data (Fig. 11) are typical of calc-alkaline suites, with a decline in total iron and a steady increase in SiO₂ with decreasing MgO contents.

As the basement lavas are to some extent altered, it is important to assess how secondary processes have affected original chemical compositions. Petrographically, the freshest samples are in the upper 20 m of Unit 1 and the most altered lavas are found in Units 3–5. The consistency of most immobile elements within the various flows of Unit 1 also suggests that these andesites are close to their unaltered compositions. The contrast between the upper and lower units of the section is paralleled by chemostratigraphic variations, particularly in the distribution of MgO, as shown in Figure 10. Units 3–5 are intercalations of basaltic andesite, andesite, and dacite/rhyolite whereas Units 1 and 2 are entirely andesite. It is, therefore, a possibility that the extremes found in the lower units are simply a function of an alteration process. Support for this comes from observations that the basaltic andesites are fractured and friable, suggesting a fluid-related density decrease, whereas the rhyolitic rocks are hard and have silicified groundmasses, commensurate with bulk silica addition.

Lavas from Hole 792E show similarly anomalous trace element features to the forearc basin basement of Hole 793B. Notably, Hole 792E lavas show large variations in P and Y (Fig. 12) not commensurate with the quantities of crystallization estimated from major element compositions. This is investigated further by comparing average analyses of basaltic andesites, andesites, and dacites. Figure 13 shows the relative enrichment/depletion of trace elements in average basaltic andesite and dacite relative to average andesite. Contrary to normal fractionation systems, the basaltic andesite has higher Zr and lower Ni and Cr compared with average andesite. Furthermore, the basaltic andesite has a factor of 2–3 less P, Y, Rb, K, and Ba. The average dacite could be derived from the andesite by fractional crystallization in light of the lower Ni and Cr. However, the dacite profile in Figure 13 has similar levels of Ti, Zr, and Sr to the basaltic andesite, combined with a relative enrichment of P, Y, and the LFS elements.

The basaltic andesites have similar phenocryst mineral proportions to the andesites, with the exception of the andesites at the top that lack quartz. As the basaltic andesites are more altered than the andesites, the possibility is raised that the basaltic andesites are simply

Table 5. Diabase sill and basalt pebble geochemistry, Hole 793B.

Core, section Interval	1R-1 1/35-39	1R-1 1/73-77	1R-1 1/115-119	1R-1 1/132-136	1R-2 2/15-19	1R-2 2/25-31	1R-2 2/61-65	1R-2 2/91-95	1R-3 3/1-5	1R-3 3/27-31	1R-3 3/77-82	3R-1 1/95-98	3R-1 1/98-100
Depth (MBSF)	586.79	587.23	587.65	587.82	588.15	588.27	588.60	588.92	589.36	589.58	590.12	605.00	605.28
Sample no.	001	002	003	004	005	006	007	008	009	010	011	S-1	012
Unit													
Lithology	Diabase	Diabase	Diabase	Diabase	Diabase	Diabase	Diabase	Diabase	Diabase	Diabase	Diabase	Basalt	Basalt
Major elements (wt%)													
SiO ₂	52.84	52.52	52.65	52.07	52.24	52.61	53.10	52.87	52.99	53.05	52.58	52.81	52.68
TiO ₂	0.58	0.52	0.57	0.53	0.53	0.58	0.58	0.56	0.59	0.61	0.56	0.66	0.65
Al ₂ O ₃	14.85	14.70	14.44	14.46	14.37	14.51	14.68	14.80	14.86	14.71	14.63	17.07	16.76
Fe ₂ O ₃ *	10.61	9.68	10.34	10.03	10.17	10.44	9.80	9.82	10.05	10.05	9.65	10.42	10.24
MnO	0.16	0.17	0.19	0.19	0.19	0.19	0.16	0.15	0.16	0.16	0.17	0.16	0.18
MgO	8.56	9.34	8.95	9.41	9.68	9.10	8.99	8.80	8.67	8.72	9.26	5.27	5.33
CaO	10.19	10.85	10.82	11.01	10.94	10.80	10.49	10.27	10.39	10.28	10.76	11.70	11.61
Na ₂ O	1.94	1.86	1.72	1.64	1.63	1.70	1.88	1.97	1.93	2.03	1.96	1.91	2.13
K ₂ O	0.26	0.11	0.27	0.26	0.20	0.18	0.32	0.32	0.36	0.34	0.28	0.30	0.34
P ₂ O ₅	0.06	0.05	0.05	0.05	0.05	0.05	0.06	0.05	0.05	0.06	0.06	0.04	0.06
(LOI)	0.48	0.37	0.20	0.55	0.46	0.33	0.30	0.53	0.25	0.36	0.68	0.33	0.00
Total	100.05	99.80	100.00	99.65	100.00	100.16	100.06	99.61	100.05	100.01	99.91	100.34	99.98
Trace elements (ppm)													
P	281	287	261	249	258	282	296	273	293	303	278		179
Zr	34.4	32.8	35.2	32.6	31.9	35.0	36.4	35.3	35.5	38.6	34.2		37.6
Y	17.9	17.2	18.4	17.4	17.2	18.4	18.1	17.3	17.9	17.7	17.7		21.1
Ga	14.9	15.4	14.7	14.9	14.2	15.1	14.9	14.8	14.8	15.1	14.4		15.9
Rb	2.8	1.8	3.6	4.1	3.6	2.9	4.3	4.2	5.8	5.5	4.8		5.1
Sr	116	119	116	113	112	117	116	117	117	116	114		140
Ba	37	52	103	45	46	64	66	55	67	50	45		32
V	288	252	284	266	261	280	277	265	280	282	290		323
Nb	0.4	0.0	0.0	0.0	0.0	0.5	0.0	0.1	0.3	0.7	0.3		0.4
Ni	76	99	93	104	113	97	100	89	92	91	106		25
Cr	167	252	225	260	249	233	255	200	220	224	275		102
Zn	69	66	72	70	70	71	73	67	72	72	72		79
Cu	58	84	109	112	84	93	99	97	95	105	88		90
Nd													
Sm													
100 Mg/Mg+Fe(t)	64.0	68.0	65.6	67.4	67.7	65.7	66.9	66.4	65.5	65.6	67.9	52.7	53.4
Al ₂ O ₃ /TiO ₂	25.6	28.3	25.3	27.3	27.1	25.0	25.3	26.4	25.2	24.1	26.1	25.9	25.8
CaO/TiO ₂	17.6	20.9	19.0	20.8	20.6	18.6	18.1	18.3	17.6	16.9	19.2	17.7	17.9
CaO/Al ₂ O ₃	0.69	0.74	0.75	0.76	0.76	0.74	0.71	0.69	0.70	0.70	0.74	0.69	0.69
Ti/Zr	101	95	97	97	100	99	96	95	100	95	98		104
Zr/Y	1.9	1.9	1.9	1.9	1.9	1.9	2.0	2.0	2.0	2.2	1.9		1.8

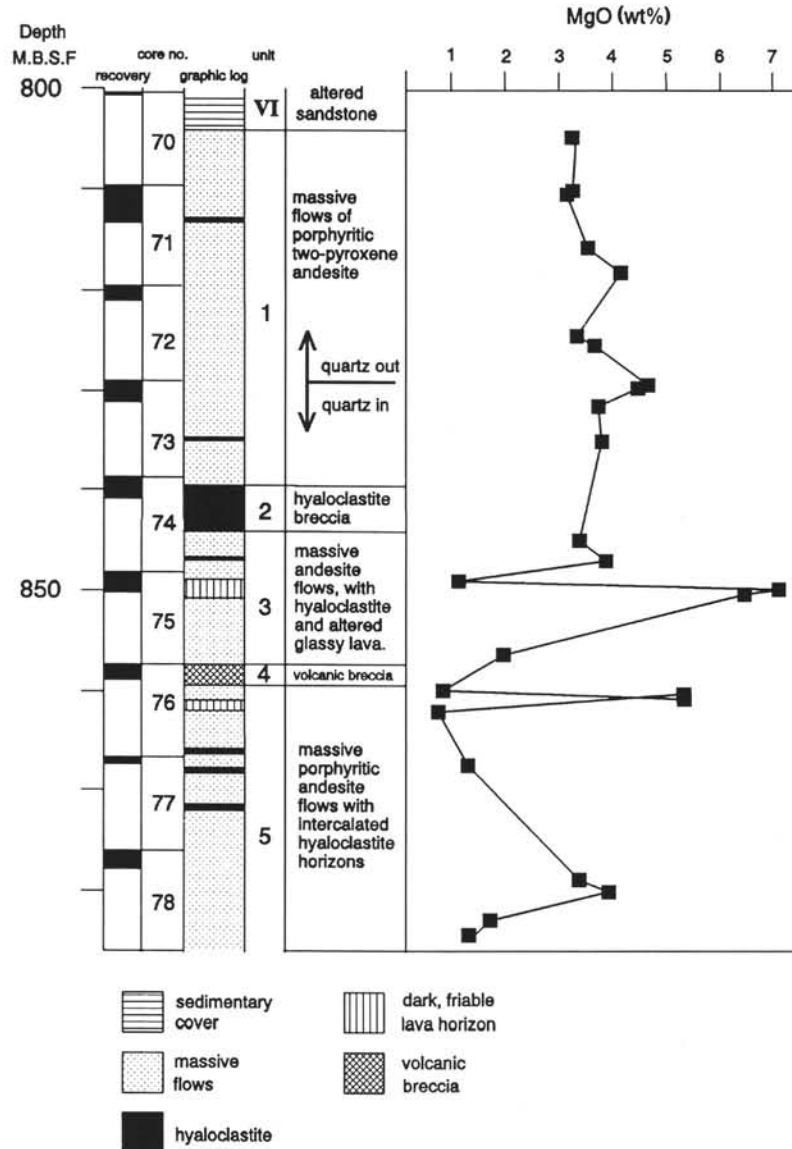


Figure 10. Stratigraphic summary of basement rock sequence in Hole 792E, Cores 126-792E-70R through -78R. Recovery within each core is proportionally expanded to fill the total core penetration. MgO values are plotted vs. depth for all samples analyzed from coherent igneous units.

andesites that have undergone hydrothermal alteration. The net result of the alteration is a decrease in silica, P, Y, and LFS elements with a resultant increase in the contents of the immobile elements Ti and Zr. Rhyolite and, to a limited extent, dacite compositions are likely to be the result of net deposition of the solute elements along particular horizons. As with the Hole 793B basement, Sr is apparently relatively stable during the leaching process and can again be explained by the retention of Sr in unaltered plagioclase.

RADIOGENIC ISOTOPE GEOCHEMISTRY OF FOREARC VOLCANICS

Basement volcanics from Holes 793B and 792E together with a sample from the Neogene intrusion in Hole 793B were analyzed for Sr, Nd, and Pb isotopes. Lead isotopes were analyzed at Royal Holloway and Bedford New College, London, using a VG354 five-collector mass-spectrometer with static data collection. Ratios were normalized for mass fractionation to SRM981 by about 0.11%/amu.

Internal errors are estimated at better than 0.005%/amu and reproducibility at better than 0.05%/amu. Sr and Nd isotopes were measured at Universite Blaise Pascal, Clermont-Ferrand, France. Pb, Nd, and Sr isotope data are presented in Table 8.

Sr-Nd Isotopes

The nine samples from Hole 793B basement have consistent $^{143}\text{Nd}/^{144}\text{Nd}$ ratios (Fig. 14), with ϵ_{Nd} ranging from 5.63 to 6.82 ($t = 30$ Ma). $^{87}\text{Sr}/^{86}\text{Sr}$ ratios are slightly more dispersed (0.7038–0.7044) indicating that basalt-seawater interaction or hydrothermal fluids have disturbed the original proportions of radiogenic Sr. However, $^{143}\text{Nd}/^{144}\text{Nd}$ ratios do not correlate with enrichment of the LFS elements or the unusual P and Y variations. This suggests that despite the apparent mobility of the REE during basement alteration, the fluids were of a similar Nd-isotopic composition to the lavas. As such, we propose that the fluids causing the redistribution of the REE obtained their REE solute from within the lava pile. If the fluids did

Table 6. Modal mineralogy of basement rocks, Hole 792E.

Sample/ analysis	Core, section, interval (cm)	Depth (mbsf)	Plag	Opx	Cpx	Qtz	Opaques
A -	71R-CC, 10	812.6	36.5	5.0	3.5	-	1.7
B	74R-1, 146	840.3	23.1	0.1	6.3	-	8.9
C	74R-1, 146	840.3	30.7	5.9	1.8	-	2.4
D S31	76R-1, 61	858.3	35.5	6.5	1.2	1.5	1.2
E S-34	78R-1, 134	877.9	32.8	6.5	4.4	1.3	1.3

Notes: All analyses performed by point counting (>400 counts per section).
Reported values are percentages, with groundmass the residual percentage.
Plag = plagioclase, Opx = orthopyroxene, Cpx = clinopyroxene, Qtz = quartz.

A = Porphyritic andesite, Unit 1
B = Basal 1.4cm-thick layer of hyaloclastite breccia, Unit 2
C = Top of andesite flow - Unit 3, directly beneath sample b.
D = Porphyritic quartz-bearing andesite, Unit 5.
E = Porphyritic quartz-bearing andesite, Unit 5.

circulate through sediments or lower regions of the basement, either they did not scavenge significant quantities of REE in these locations, or these lithologies had similar $^{143}\text{Nd}/^{144}\text{Nd}$ systematics.

In comparison to other lavas in Izu-Bonin arc-trench system (Fig. 14), the Hole 793B basement has lower ϵ_{Nd} than MORB and the active arc, and it lies at the upper end of the spectrum of boninites from the Izu-Bonin outer-arc high.

Pb Isotopes

Lead isotopes were measured on six samples from Hole 793B basement, three samples from Hole 792E, and one sample from the Neogene diabase sill in Hole 793B. Figures 15 and 16 compare $^{207/204}\text{Pb}$ - $^{206/204}\text{Pb}$ and $^{208/204}\text{Pb}$ - $^{206/204}\text{Pb}$ data from Leg 126 with analyses from potential components and lavas from the western Pacific environs. Lavas from the forearc basement at Sites 792 and 793 lie within the range of isotopic compositions of Pacific MORB, on or slightly above the Northern Hemisphere reference line ($\Delta 7/4$ and $\Delta 8/4$ values range from -1.74 to 3.3 and 7.3 to 37.4, respectively). The diabase sill lies between the Pacific MORB and western Pacific sediment fields on both $^{207/204}\text{Pb}$ - $^{206/204}\text{Pb}$ and $^{208/204}\text{Pb}$ - $^{206/204}\text{Pb}$ plots ($\Delta 7/4$ and $\Delta 8/4$ are 7.2 and 52.4, respectively).

Unlike the Bonin Islands (Dobson and Tilton, 1989), no clear evidence for a $^{207/204}\text{Pb}$ -rich sedimentary component was found in the basement lavas of the forearc basin. However, the $^{207/204}\text{Pb}$ datum from the diabase sill (Fig. 15 and 16) suggests that sediments may have played a role in its petrogenesis. Contamination of the sill magma could have taken place either in the mantle source by introduced slab sediments or by digestion of host sediments during intrusion. The lack of available Pb data for Izu arc lavas of comparable composition as well as intruded sedimentary horizons precludes an interpretation regarding the nature of contamination.

PETROGENETIC RELATIONS BETWEEN ARC-TRENCH MAGMAS

The occurrence of boninite series volcanics (BSV) in the forearc terrains of the Western Pacific has been well documented (e.g., Dietrich et al., 1978; Hickey and Frey, 1982; Umino, 1986; Bloomer and Hawkins, 1987). However, the question remains as to whether the current location of boninite lavas bears any relation to their original position with respect to the subduction zone and arc. Drilling during Leg 126 sampled igneous units within the forearc region

which, combined with age constraints, suggest that the boninites were generated within current tectonic framework.

The Hole 793B diabase sill is younger than about 12 Ma and was recovered from the center of the forearc basin. However, its similar composition to Torishima and other Izu arc volcanoes, together with the possibility of lateral injection from the arc, do not allow this intrusion to be constrained as forearc volcanism. Age relations between basement at Sites 792 and 793 do provide an insight into the temporal development of the arc-trench crust. The calc-alkaline volcanic edifice drilled at Site 792, combined with the seismic evidence, demonstrates that during the Oligocene (about 30-33 Ma) a well-developed arc-chain existed in a similar orientation to the modern arc. Basement lavas from Hole 793B, trenchward of Site 792, are interpreted as being in the age range from 26 to 33 Ma, (Taylor and Mitchell, this volume). These lavas were clearly produced in a forearc environment in response to basin formation between arc and outer-arc high. As such, Site 793B basement represents one of the few well-constrained examples of forearc volcanism.

Comparable tectonic structures and age relationships along the length of the Izu and Mariana subduction systems suggest that little tectonic erosion has taken place between the outer-arc high and trench in the duration of this subduction system. The absence of thrust-related structures across the arc suggests that tectonic units within the forearc have not been juxtapositioned. Hence, it is likely that the outer-arc high lavas were also generated in a forearc location.

In light of the consistent relative positions between tectonic units, Taylor et al. (1992) examined spatial geochemical variations within the Izu-Bonin arc-trench region. These authors found that indexes of mantle depletion (e.g., TiO_2 , Y, and $\text{Al}_2\text{O}_3/\text{TiO}_2$) displayed a gradual transition from the arc toward the trench. Figure 17 shows the decline in TiO_2 contents of lavas from the backarc to the forearc, reflecting a more depleted mantle source toward the trench. On the active arc, the lowest-Ti lavas are primitive island arc tholeiites, similar to the Hole 793B diabase intrusion (about 0.5 wt% TiO_2 at 9 wt% MgO). In the forearc rift-basin, basement lavas are low-Ti tholeiites transitional to boninites (0.3 wt% TiO_2 at 9 wt% MgO). Boninitic volcanics closest to the trench have the lowest TiO_2 concentrations (0.15 wt%). This lateral variation in geochemistry can be related to a compositionally stratified mantle combined with variable melting location in response to slab depth (Taylor et al., 1992).

Lavas from the Izu-Bonin forearc basin are transitional between arc tholeiites and boninites in terms of their petrography and trace element depletion. However, an important char-

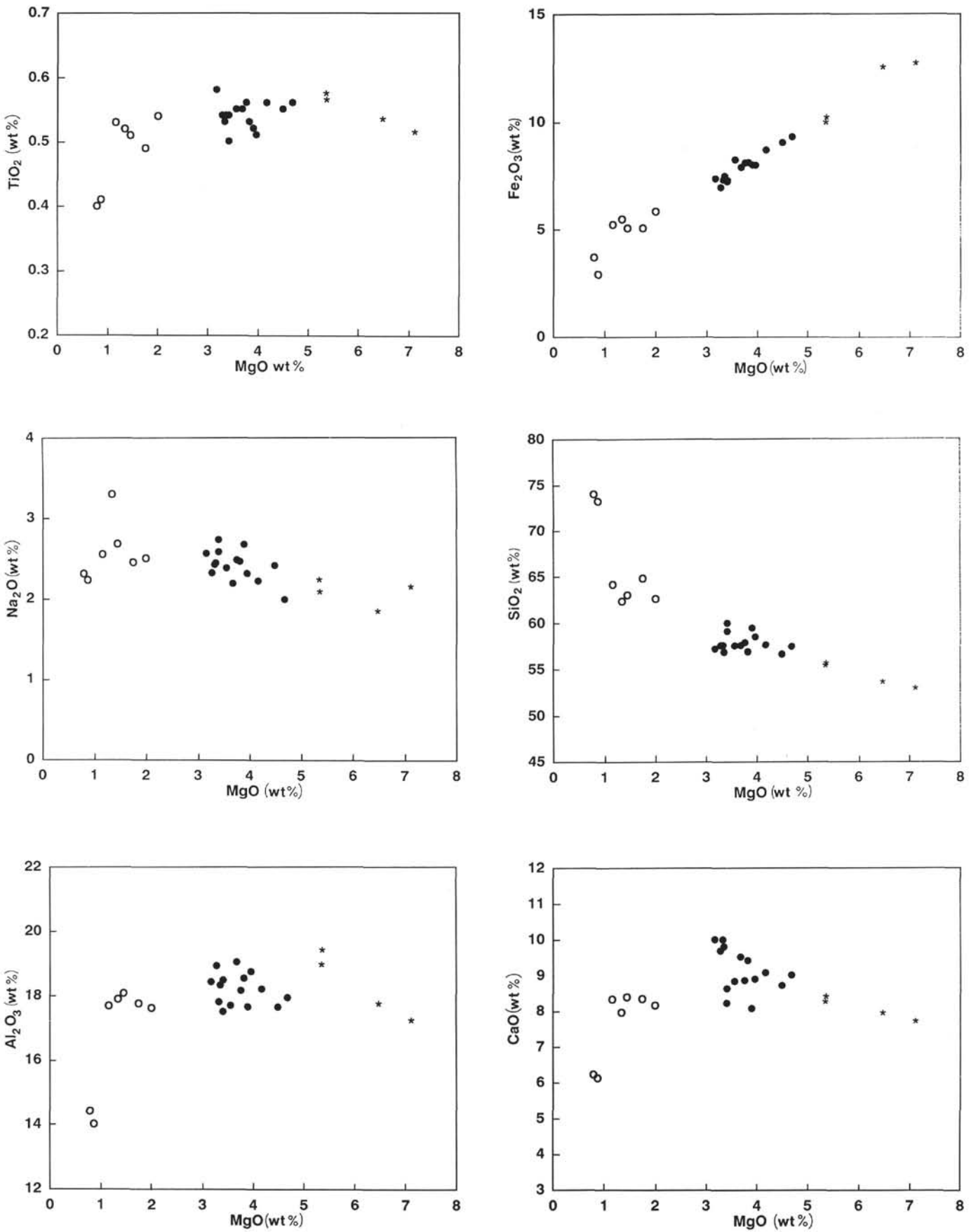


Figure 11. Major elements plotted vs. MgO for Hole 792E basement (all values in wt%).

Table 7. Basement geochemistry, Hole 792E.

Core, section	70R-cc	71R-1	71R-1	71R-2	71R-3	72R-1	72R-1	73R-1	73R-1	73R-1	73R-2	73R-2	74R-2	75R-1	75R-1
Interval	16-20	9-13	18-21	89-92	34-38	100-104	111-115	15-18	18-21	72-76	3-7	53-57	104-108	18-22	49-51
Depth (MBSF)	805.00	810.00	810.38	815.66	818.20	824.59	825.50	829.50	829.84	831.60	835.12	845.00	847.10	849.11	850.00
Sample no.	099	S-24	100	101	S-25	103	S-26	S-27	104	105	106	S-28	110	112	113
Unit	1	1	1	1	1	1	1	1	1	1	1	3	3	3	3
Lithology	Andesite	Dacite	Bas.and												
Major elements (wt%)															
SiO ₂	57.47	57.48	57.12	57.44	57.55	56.77	57.48	57.39	56.55	57.79	56.83	59.91	59.39	64.20	52.57
TiO ₂	0.53	0.54	0.58	0.55	0.56	0.54	0.55	0.56	0.55	0.56	0.53	0.54	0.52	0.53	0.51
Al ₂ O ₃	17.80	18.92	18.42	17.69	18.20	18.32	19.04	17.93	17.64	18.15	18.53	17.50	17.65	17.70	17.15
Fe ₂ O ₃ *	7.26	6.90	7.31	8.19	8.65	7.42	7.84	9.26	8.99	8.05	8.07	7.17	7.95	5.24	12.56
MnO	0.31	0.15	0.25	0.32	0.14	0.13	0.08	0.10	0.13	0.13	0.18	0.05	0.09	0.09	0.17
MgO	3.33	3.28	3.17	3.56	4.17	3.35	3.68	4.68	4.49	3.76	3.82	3.41	3.90	1.16	7.11
CaO	9.98	9.67	9.99	8.82	9.06	9.79	9.50	8.99	8.70	8.84	9.40	8.21	8.06	8.34	7.63
Na ₂ O	2.41	2.31	2.55	2.37	2.21	2.43	2.18	1.98	2.40	2.47	2.45	2.57	2.66	2.55	2.10
K ₂ O	0.19	0.23	0.28	0.55	0.15	0.18	0.13	0.14	0.16	0.20	0.17	0.20	0.17	0.28	0.17
P ₂ O ₅	0.15	0.11	0.11	0.07	0.05	0.47	0.13	0.04	0.06	0.06	0.09	0.04	0.06	0.09	0.03
(LOI)	1.77	1.01	0.96	0.93	0.81	1.26	1.05	1.10	0.98	0.53	1.30	1.44	1.17	0.72	1.71
Total	99.43	99.59	99.78	99.56	100.74	99.40	100.61	101.07	99.67	100.01	100.07	99.60	100.45	100.18	100.00
Trace elements (ppm)															
P	635		444	281		2244			256	257	376		227	355	92
Zr	39.2	39.9	41.1	39.0	39.9	40.4	42.2	41.4	41.1	41.8	41.1	38.7	41.7	41.8	45.3
Y	24.5	20.3	25.7	20.8	20.3	46.8	28.1	21.8	22.8	22.5	25.0	18.4	23.7	27.2	7.2
Ga	16.0		15.8	15.8		16.3			16.0	15.8	15.8		15.8	16.0	14.2
Rb	3.0	1.4	3.3	10.3	1.4	3.1	1.2	1.3	3.1	3.1	3.4	2.4	3.6	4.3	2.8
Sr	172	176	175	166	176	185	188	175	170	170	177	166	167	160	180
Ba	18	31	26	24	31	24	16	12	19	26	10	28	15	24	391
V	249	258	267	251	258	253	260	244	248	254	237	242	197	243	162
Nb	0.0	0.9	0.1	0.2	0.9	0.2	1.3	1.1	0.0	0.3	0.1	0.6	0.0	0.0	0.6
Ni	12	9	12	12	9	11	9	9	13	12	11	6	10	6	8
Cr	27	12	29	26	12	66	11	12	97	63	20	0	10	19	18
Zn	58	86	74	16	86	66	82	93	73	72	66	79	79	63	109
Cu		34			34		28	27				39			
Nd															
Sm															
100 Mg/Mg+Fe(t)	50.2	51.1	48.8	48.9	51.5	49.8	50.8	52.7	52.4	50.7	51.0	51.1	51.9	32.8	55.5
Al ₂ O ₃ /TiO ₂	33.6	35.0	31.8	32.2	32.5	33.9	34.6	32.0	32.1	32.4	35.0	32.4	33.9	33.4	33.6
CaO/TiO ₂	18.8	17.9	17.2	16.0	16.2	18.1	17.3	16.1	15.8	15.8	17.7	15.2	15.5	15.7	15.0
CaO/Al ₂ O ₃	0.56	0.51	0.54	0.50	0.50	0.53	0.50	0.50	0.49	0.49	0.51	0.47	0.46	0.47	0.44
Ti/Zr	81	81	85	85	84	80	78	81	80	80	77	84	75	76	67
Zr/Y	1.6	2.0	1.6	1.9	2.0	0.9	1.5	1.9	1.8	1.9	1.6	2.1	1.8	1.5	6.3

Table 7 (continued).

Core, section interval	75R-1	75R-2	76R-1	76R-1	76R-1	76R-1	77R-1	78R-1	78R-1	78R-1	78R-1
Interval	50-55	69-73	43-46	60-64	64-68	85-87	3-7	71-74	80-85	131-136	132-135
Depth (MBSF)	850.50	856.56	860.10	861.00	860.52	862.20	867.57	879.00	880.20	883.00	884.50
Sample no.	S-29	114	S-30	S-31	116	S-32	117	118	S-33	S-34	119
Unit	3	3	5	5	5	5	5	5	5	5	5
Lithology	Bas.and	Dacite	R.dacite	Bas.and	Bas.and	R.dacite	Dacite	Andesite	Andesite	Dacite	Dacite
Major elements (wt%)											
SiO ₂	53.26	62.67	73.24	55.28	55.05	74.04	62.39	59.02	58.41	64.87	63.06
TiO ₂	0.53	0.54	0.41	0.56	0.57	0.40	0.52	0.50	0.51	0.49	0.51
Al ₂ O ₃	17.66	17.63	14.03	19.32	18.87	14.43	17.91	18.48	18.74	17.77	18.09
Fe ₂ O ₃ *	12.37	5.84	2.92	10.04	9.81	3.72	5.49	7.22	7.94	5.08	5.08
MnO	0.16	0.07	0.02	0.14	0.16	0.02	0.06	0.08	0.07	0.03	0.06
MgO	6.47	2.00	0.87	5.36	5.35	0.79	1.34	3.41	3.96	1.75	1.45
CaO	7.85	8.17	6.13	8.31	8.17	6.23	7.97	8.61	8.88	8.35	8.40
Na ₂ O	1.80	2.50	2.23	2.04	2.19	2.31	3.30	2.72	2.30	2.45	2.68
K ₂ O	0.12	0.16	0.24	0.14	0.20	0.22	0.48	0.17	0.14	0.37	0.40
P ₂ O ₅	0.02	0.09	0.06	0.02	0.04	0.04	0.06	0.10	0.04	0.17	0.18
(LOI)	2.23	0.90	1.28	3.10	2.27	1.49	0.00	0.38	1.62	0.69	0.00
Total	100.24	99.67	100.15	101.21	100.41	102.20	99.52	100.31	100.99	101.33	99.91
Trace elements (ppm)											
P		368			136		268	422			661
Zr	43.8	42.3	34.7	48.7	53.8	35.7	43.1	45.2	43.7	42.3	41.6
Y	5.9	26.0	15.4	6.9	7.3	22.4	21.1	19.2	10.3	30.6	29.2
Ga		16.2			15.7		16.6	16.0			16.2
Rb	1.6	3.6	2.7	2.1	3.4	3.1	6.0	3.3	1.2	3.9	6.1
Sr	155	165	134	166	159	138	173	167	170	162	163
Ba	33	23	42	2	0	211	41	15	6	43	36
V	186	235	153	247	216	125	338	205	260	233	225
Nb	0.5	0.1	1.4	0.7	0.3	1.0	0.4	0.0	0.7	1.2	0.6
Ni	5	8	0	7	9	4	6	9	5	4	7
Cr	0	16	0	2	31	2	22	20	8	4	25
Zn	134	58	41	98	71	78	50	63	80	55	40
Cu	18		26	17		31			28	18	
Nd											
Sm											
100 Mg/Mg+Fe(t)	53.5	43.0	39.6	54.0	54.6	31.9	34.9	51.0	52.3	43.1	38.6
Al ₂ O ₃ /TiO ₂	33.3	32.6	34.2	34.5	33.1	36.1	34.4	37.0	36.7	36.3	35.5
CaO/TiO ₂	14.8	15.1	15.0	14.8	14.3	15.6	15.3	17.2	17.4	17.0	16.5
CaO/Al ₂ O ₃	0.44	0.46	0.44	0.43	0.43	0.43	0.45	0.47	0.47	0.47	0.46
Ti/Zr	73	77	71	69	64	67	72	66	70	69	73
Zr/Y	7.4	1.6	2.3	7.1	7.4	1.6	2.0	2.4	4.2	1.4	1.4

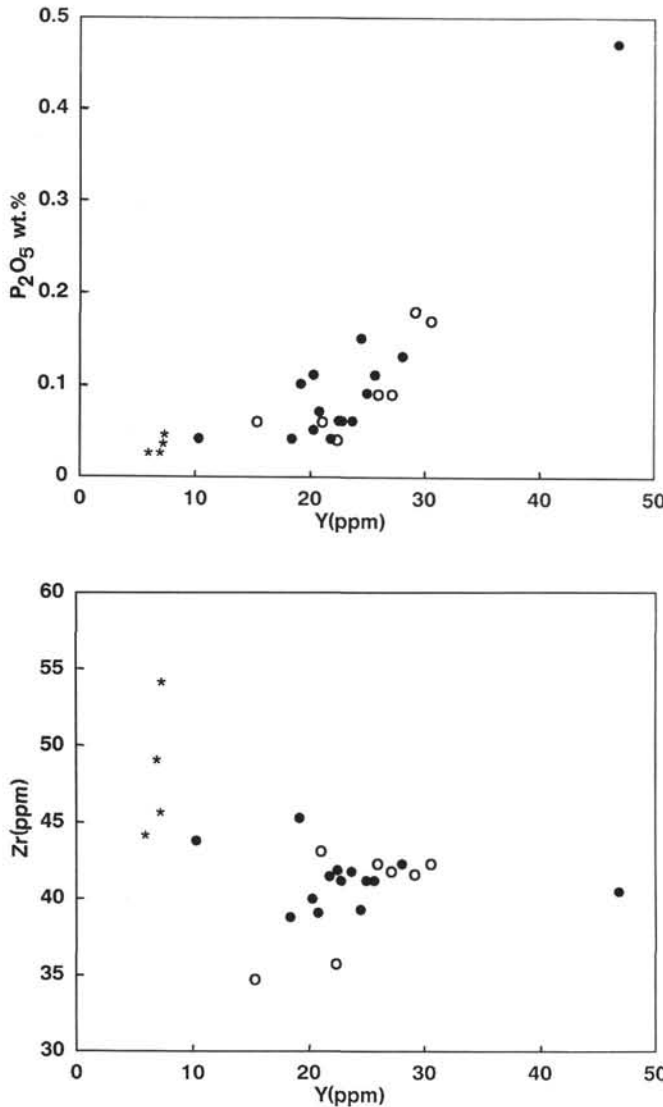


Figure 12. P₂O₅ and Zr plotted vs. Y for Hole 792E basement.

acteristic of boninitic volcanism is the nature of enrichments to their source. Figure 18 combines two parameters that distinguish boninites from arc and oceanic basalt compositions. Western Pacific boninites have lower Ti/Zr ratios and ϵ_{Nd} compared with MORB and lavas from the active Izu-Mariana arcs. These features have been ascribed to enrichment in light REE and Zr relative to middle/heavy REE, Ti, and Y (Sun and Nesbitt, 1978; Hickey and Frey, 1982; Cameron, 1985;

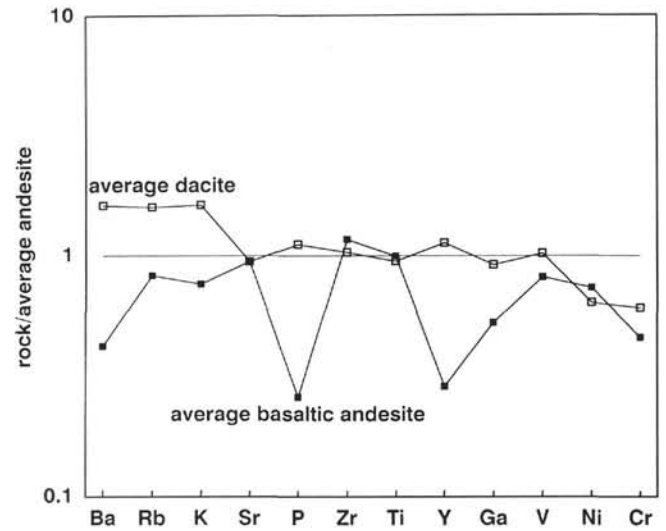


Figure 13. Average trace element compositions for average dacite (Unit 5) and average basaltic andesite (Unit 5) normalized to average andesite (Unit 1).

Taylor and Nesbitt, 1988). Samples from the Hole 793B basement are intermediate between arc and boninite in terms of both parameters in Figure 18.

It is notable that the Site 793 lavas are geochemically very similar to Site 458 bonzite andesites from the Mariana forearc basin. Lavas from both these sites are intermediate in composition between respective active arc and outer-arc high lavas (e.g., Fig. 18). This is taken to reflect their similar tectonic setting (forearc basin) and age (Hussong, Uyeda, et al., 1981; Taylor and Mitchell, this volume). Geochemical transects across the Izu-Bonin and Mariana arcs demonstrate a shallower source for the basin volcanics relative to the arc volcanics (Taylor et al., 1992), and a parallel mantle evolution along the length of the Izu-Mariana system.

CONCLUSIONS

Drilling during Leg 126 determined the composition and nature of lavas within the Izu-Bonin forearc basin. Basement at the center of the basin (Site 793) consists of Oligocene synrift volcanics. These are two-pyroxene basaltic andesites, with HFSE contents lower than the active Izu arc. On the western edge of the forearc basin (Site 792), lavas were recovered from a basement promontory, postulated as a relict arc volcano. The volcanics from this site are massive flows and breccias of two-pyroxene andesite and dacite with calc-alkaline affinities.

At Site 793, basement lavas show anomalous behavior of P, Y, and REE relative to HFS elements. These can be attributed to post-eruptive fluid-rock interaction, which redistributed P, Y, and REE within the basement system. Similar discrepancies are found in the Site 792 lavas,

Table 8. Nd, Sr, and Pb isotopic results from Hole 793B.

Core Interval Sample number Lithology	1R-2 61-65 007 diabase	86R-1 128-131 020 cpx-bas	88R-1 65-68 S-8 aph bas	92R-2 70-74 030 cpx-pill	92R-3 25-28 S-10 cpx-pill	97R-1 124-127 S-13 cpx-pill	99R-1 54-55 S-14 cpx-pill	104R-1 65-70 053 cpx-pill	104R-2 49-54 S-18 cpx-pill	104R-2 69-75 055 cpx-pill	105R-1 127-131 S-17 cpx-pill	110R-1 1-3 S-19 c-spot	111R-1 110-115 079 cpx mas	112R-1 59-63 S-20 cpx mas	113R-3 137-141 S-21 aph bas	113R-4 35-41 088 aph bas
Sr	116	129	156	135	163	140	140	161	178	201	129	147	152	187	196	195
Nd			4.64		5.92	2.46	3.69		5.61		2.77	3.46		3.28	7.36	
Sm			1.48		1.73	0.84	1.21		1.78		0.97	1.06		1.04	2.32	
^{143/144} Nd			0.51296		0.51296	0.51296	0.51295		0.51299		0.51303	0.61296		0.51296	0.51297	
^{87/86} Sr			0.70377		0.70410	0.70384	0.70397		0.70383		0.70394	0.70383		0.70439	0.70389	
ϵ_{Nd}			6.4		6.4	6.2	6.1		6.8		5.6	6.3		6.2	6.5	
^{206/204} Pb	18.35	18.20		18.18				18.22		18.21			18.16		18.17	
^{207/204} Pb	15.56	15.49		15.46				15.48		15.47			15.47		15.44	
^{206/204} Pb	38.33	37.93		37.81				37.91		37.87			37.84		37.80	

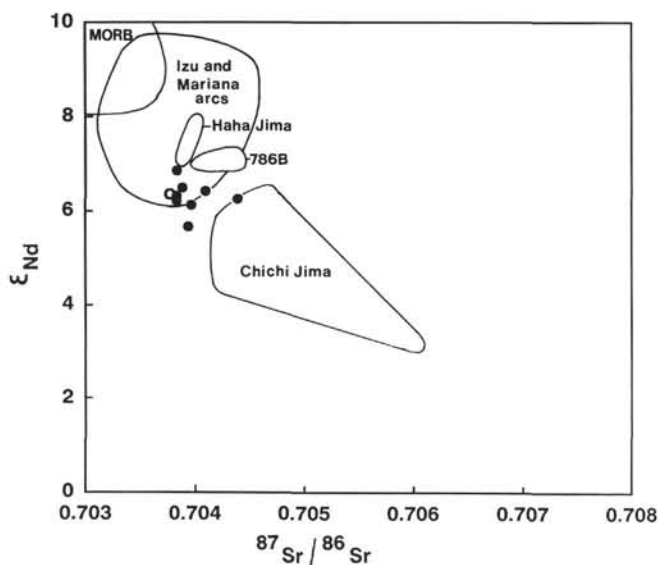


Figure 14. ϵ_{Nd} plotted vs. $^{87}Sr/^{86}Sr$ for Hole 793B basement. Fields for Izu and Mariana arcs from Woodhead (1989) and Nohda and Wasserburg (1981); ODP Leg 125 fields for Hole 786B from Pearce et al. (1992); and Chichi Jima and Haha Jima from Taylor, Nesbitt, and Vidal (unpubl. data).

with more extreme element redistribution. Groundmass changes and fluid movements have produced SiO_2 -rich and SiO_2 -poor meta-andesites with characteristic concentration and dilution of HFS elements.

Age relationships of basement lavas from the two forearc Sites (792 and 793) indicate that lavas from the forearc basin are younger than the Oligocene arc at Site 792. This demonstrates that the current Izu-Bonin forearc crust was in a forearc location during Oligocene rifting and experienced synrift volcanism.

Trace element and isotopic evidence indicates that the Hole 793B basement volcanics are transitional between arc-tholeiite and boninite chemistry. This suggests that their intermediate location between the outer-arc high (boninitic) and the active arc (arc-tholeiite) can be related to a gradual change in melting environment toward the trench.

ACKNOWLEDGMENTS

This work was supported by Natural Environment Research Council Grant No. GST/02/416 (RNT and RWN). RNT would like to thank all Leg 126 participants for a good cruise, and I. Chaplin for rock preparation logistics. The reviewers are thanked for their helpful and constructive comments.

REFERENCES

- Bienvenu, P., Bougault, H., Joron, J. L., Treuil, M., and Dmitriev, L., 1990. MORB alteration: rare-earth element/non-rare-earth hygromagmaphile element fractionation. *Chem. Geol.*, 82:1–14.
- Bloomer, S. H., and Hawkins, J. W., 1987. Petrology and geochemistry of boninite series volcanic rocks from the Mariana trench. *Contrib. Mineral. Petrol.*, 97:361–377.
- Cameron, W. E., 1985. Petrology and origin of primitive lavas from the Troodos ophiolite, Cyprus. *Contrib. Mineral. Petrol.*, 89:239–255.
- Croudace, I. W., and Gilligan, J., 1990. Versatile and accurate trace element determinations in iron-rich and other geological samples using X-ray fluorescence analysis. *X-ray Spectrom.*, 19:117–123.
- Croudace, I. W., and Marshall, S., 1991. Determination of rare-earth elements and yttrium in nine geochemical reference samples using a novel group separation procedure involving mixed acid elution ion-exchange chromatography. *Geostand. Newsl.*, 15:139–144.
- Dietrich, V., Emmermann, R., Oberhänsli, R., and Puchelt, H., 1978. Geochemistry of basaltic and gabbroic rocks from the west Mariana basin and the Marina trench. *Earth Planet. Sci. Lett.*, 39:127–144.

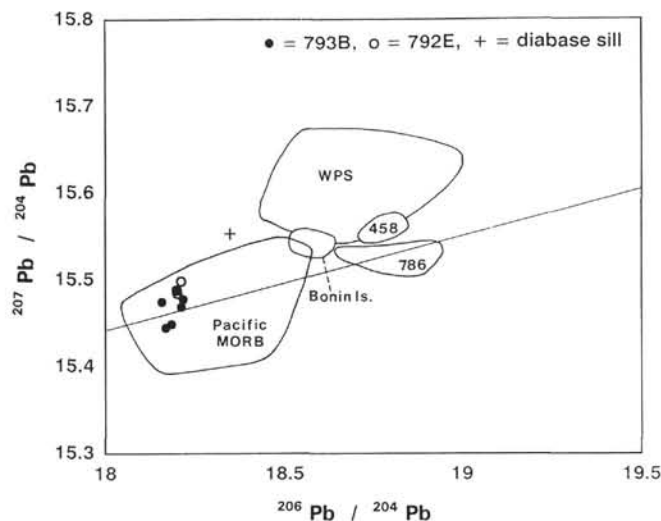


Figure 15. $^{207}Pb/^{204}Pb$ – $^{206}Pb/^{204}Pb$ for Leg 126 igneous rocks. Fields are shown for Pacific MORB (Tatsumoto, 1978; Vidal and Clauer, 1981); western Pacific sediment (WPS; Sun, 1980; Meijer, 1976; Woodhead and Fraser, 1985); Bonin islands (Taylor et al., unpubl. data); DSDP Site 458 (Hickey-Vargas, 1989); and ODP Site 786 (Pearce et al., 1992).

- Dobson, P. F., and Tilton, G. R., 1989. Th, U, and Pb systematics of boninite series volcanic rocks from Chichi-Jima, Bonin Islands, Japan. In Crawford, A. J. (Ed.), *Boninites and Related Rocks*: London (Unwin Hyman), 396–415.
- Egeberg, P. K., and Leg 126 Shipboard Scientific Party, 1990. Unusual composition of pore-waters found in the Izu-Bonin fore-arc sedimentary basin. *Nature*, 344:215–218.
- Fryer, P., Pearce, J. A., Stokking, L. B., et al., 1990. *Proc. ODP, Init. Repts.*, 125: College Station, TX (Ocean Drilling Program).
- Henderson, P., 1982. *Inorganic Geochemistry*: Oxford (Pergamon Press).
- Hickey, R. L., and Frey, F. A., 1982. Geochemical characteristics of boninite series volcanics: implications for their source. *Geochim. Cosmochim. Acta*, 46:2099–2115.
- Hickey-Vargas, R. L., 1989. Boninites and tholeiites from DSDP Site 458, Mariana forearc. In Crawford, A. J. (Ed.), *Boninites and Related Rocks*: London (Unwin Hyman), 339–356.
- Honza, E., and Tamaki, K., 1985. The Bonin Arc. In Nairn, A.E.M., Stehli, F. G., and Uyeda, S. (Eds.), *The Ocean Basins and Margins* (Vol. 7): New York (Plenum), 459–502.
- Kay, R. W., and Gast, P. W., 1973. The rare-earth content and origin of alkali-rich basalts. *J. Geol.*, 81:653–682.
- Leg 126 Shipboard Scientific Party, 1989a. Arc volcanism and rifting. *Nature*, 342:18–20.
- , 1989b. ODP Leg 126 drills the Izu-Bonin Arc. *Geotimes*, 34:36–38.
- Meijer, A., 1976. Pb and Sr isotopic data bearing on the origin of volcanic rocks from the Mariana island-arc system. *Geol. Soc. Am. Bull.*, 87:358–369.
- Nohoda, S., and Wasserburg, G. J., 1981. Nd and Sr isotopic study of volcanic rocks from Japan. *Earth Planet. Sci. Lett.*, 52:264–276.
- Pearce, J. A., Thirlwall, M., Ingram, G., Murton, B. J., Arculus, R. J., and Van Der Lann, S. R., 1992. Isotopic evidence for the origin and evolution of the Izu-Ogasawara forearc at Sites 782 and 786. In Fryer, P., Pearce, J. A., Stokking, L. B., et al., *Proc. ODP, Sci. Results*, 125: College Station, TX (Ocean Drilling Program).
- Saunders, A. D., Tarney, J., Marsh, N. G., and Wood, D. A., 1980. Ophiolites as ocean crust or marginal basin crust: a geochemical approach. In Panayiotou, A. (Ed.), *Ophiolites*: Geol. Surv. Dept Cyprus, 193–204.
- Shipboard Scientific Party, 1990. Sites 788/789. In Taylor, B., Fujioka, K., et al., *Proc. ODP, Init. Repts.*, 126: College Station, TX (Ocean Drilling Program), 97–126.
- Sun, S.-S., 1980. Lead isotopic study of young volcanic rocks from mid-ocean ridges, ocean islands and island arcs. *Philos. Trans. R. Soc. London, Ser. A*, 297:409–445.
- Sun, S.-S., and Nesbitt, R. W., 1978. Geochemical regularities and genetic significance of ophiolitic basalts. *Geology*, 6:689–693.

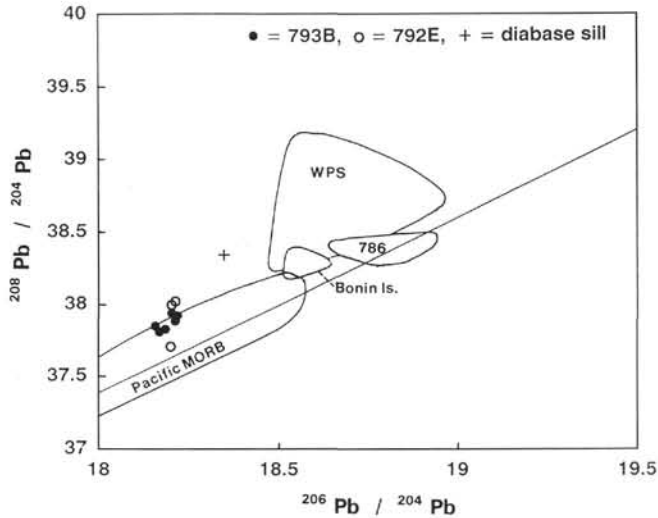


Figure 16. $^{208}\text{Pb}/^{204}\text{Pb}$ - $^{206}\text{Pb}/^{204}\text{Pb}$ for Leg 126 igneous rocks. Fields as for Figure 15.

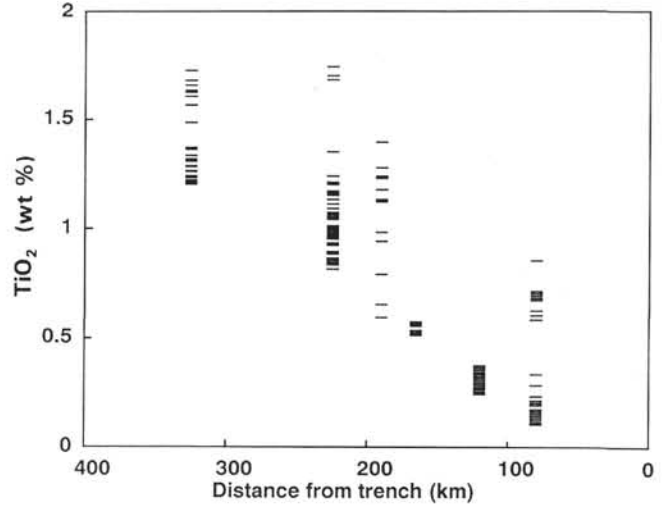


Figure 17. TiO_2 content of lavas from the Izu-Bonin arc-trench system plotted vs. distance from the trench. Details of samples used and locations are given in Taylor et al. (1992).

Tatsumoto, M., 1978. Isotopic composition of lead in oceanic basalt and its implication to mantle evolution. *Earth Planet. Sci. Lett.*, 38:63-87.

Taylor, B., Fujioka, K., et al., 1990. *Proc. ODP, Init. Repts.*, 126: College Station, TX (Ocean Drilling Program).

Taylor, B., Moore, G., Klaus, A., Systrom, M., Cooper, P., and MacKay, M., 1990. Multichannel seismic survey of the central Izu-Bonin Arc. In Taylor, B., Fujioka, K., et al., *Proc. ODP, Init. Repts.*, 126: College Station, TX (Ocean Drilling Program), 51-60.

Taylor, R. N., Murton, B. J., and Nesbitt, R. W., 1992. Chemical transects across intra-oceanic arcs: implications for the tectonic setting of ophiolites. *Spec. Publ., Geol. Soc. London*, 60:117-132.

Taylor, R. N., and Nesbitt, R. W., 1988. Light rare-earth enrichment of supra-subduction-zone mantle: evidence from the Troodos ophiolite, Cyprus. *Geology*, 16:448-451.

Umino, S., 1986. Geological and petrological study of boninites and related rocks from Chichi Jima, Bonin Islands [Ph.D. thesis]. Univ. Tokyo.

Vidal, P., and Clauer, N., 1981. Pb and Sr isotopic systematics of some basalts and sulphides from the East Pacific Rise at 21°N (Project RITA). *Earth Planet. Sci. Lett.*, 55:237-246.

Woodhead, J. D., 1989. Geochemistry of the Mariana arc (western Pacific): source composition and processes. *Chem. Geol.*, 76:1-24.

Woodhead, J. D., and Fraser, D. G., 1985. Pb, Sr, and ^{10}Be isotopic studies of volcanic rocks from the Northern Mariana Islands: implications for magma genesis and crustal recycling in the western Pacific. *Geochim. Cosmochim. Acta*, 49:1925-1930.

Date of initial receipt: 26 December 1990
 Date of acceptance: 30 September 1991
 Ms 126B-146

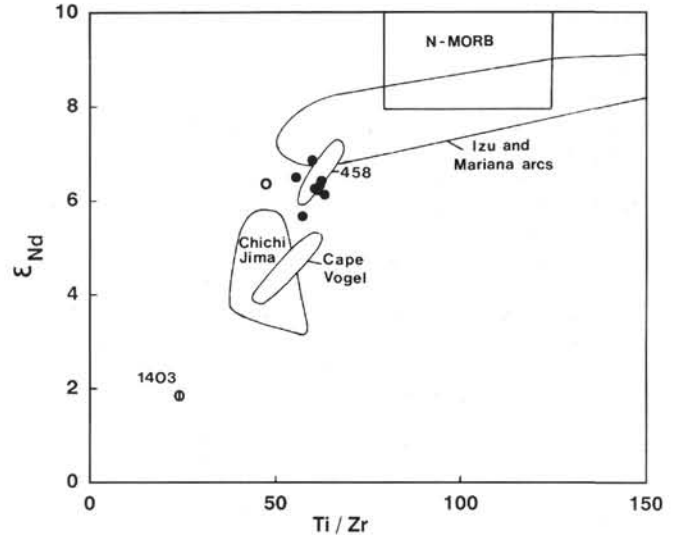


Figure 18. Ti/Zr plotted vs. ϵ_{Nd} for Hole 793B basement. Data fields for Izu and Mariana arcs from Nohda and Wasserburg (1981) and Woodhead (1989). Site 458, Site 1403, and Cape Vogel from Hickey and Frey (1982). Chichi Jima from Taylor, Nesbitt, and Vidal (unpubl. data).



Plate 1. Photomicrograph from Sample 126-793B-110R-1, 1 cm (S-19); width of field = 7 mm; cross-polarized light; basaltic andesite massive flow (Unit 13). Euhedral phenocrysts of orthopyroxene (upper right) and clinopyroxene (center left) set in a groundmass of altered glass and plagioclase microlites. Vesicles (dark patches) are coated with smectite.

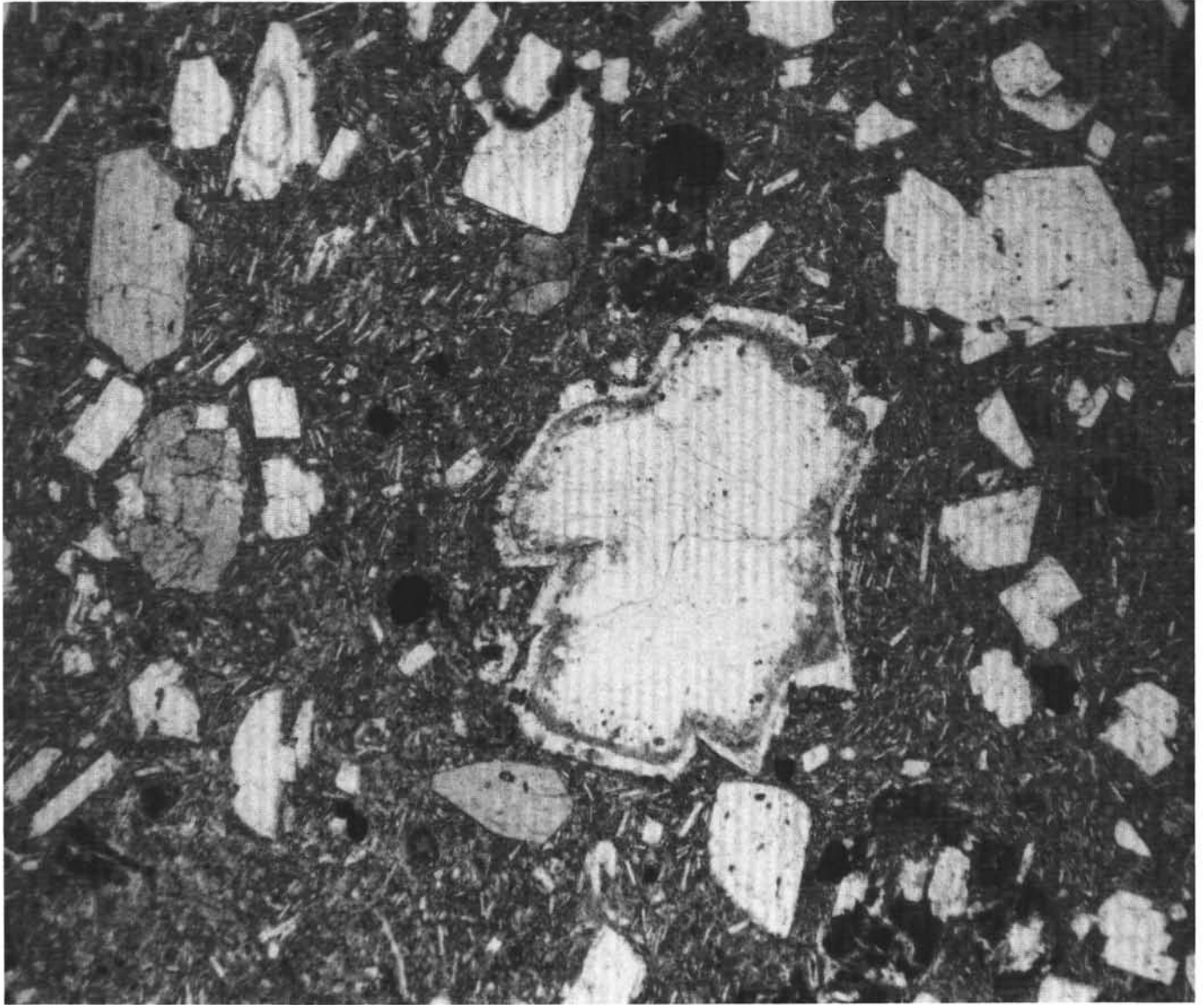


Plate 2. Photomicrograph from Sample 126-792E-71R-3, 51 cm; width of field = 6 mm; plane polarized light; typical texture in a two-pyroxene andesite from Hole 792E basement. Large plagioclase with fluid/melt inclusion zone occupies center of field. Other phenocrysts include clinopyroxene (center left) and orthopyroxene pseudomorphs (lower right).